Incorporating a root water uptake model based on the hydraulic architecture approach in terrestrial systems simulations

Mauro Sulis[1*], Valentin Couvreur[2], Jessica Keune[3], Gaochao Cai[4,5], Ivonne Trebs[1], Juergen Junk[1], Prabhakar Shrestha[6], Clemens Simmer[6,8], Stefan J. Kollet[7,8], Harry Vereecken[7,8], Jan Vanderborght[7,8]

[1] Luxembourg Institute of Science and Technology, Environmental Research and Innovation, Luxembourg

[2] Earth and Life Institute, Université catholique de Louvain, Belgium

[3] Laboratory of Hydrology and Water Management, Ghent University, Belgium

[4] Chair of Soil Physics, University of Bayreuth, Bayreuth, Germany

[5] Department of Biogeochemistry of Agroecosystems, Georg-August University of Göttingen, Göttingen, Germany

[6] Meteorological Institute, University of Bonn, Bonn, Germany

[7] Institute of Bio- and Geosciences (IBG-3), Agrosphere, Forschungszentrum Jülich, Jülich, Germany

[8] Centre for High-Performance Scientific Computing in Terrestrial Systems, Geoverbund ABC/J, Jülich, Germany

* Corresponding author: mauro.sulis@list.lu

Abstract

A detailed representation of plant hydraulic traits and stomatal closure in land surface models (LSMs) is a prerequisite for improved predictions of ecosystem drought response. This work presents the integration of a macroscopic root water uptake (RWU) model based on the hydraulic architecture approach in the LSM of the Terrestrial Systems Modeling Platform. The novel RWU approach is based on three parameters derived from first principles that describe the root system equivalent conductance, the compensatory RWU conductance, and the leaf water potential at stomatal closure, which defines the water stress condition for the plants. The developed RWU model intrinsically accounts for changes in the root density as well as for the simulation of the hydraulic lift process. The standard and the new RWU approach are compared by performing point-scale simulations for cropland over a sheltered minirhizotron facility in Selhausen, Germany, and validated against transpiration fluxes estimated from sap flow and soil water content measurements at different depths. Numerical sensitivity experiments are carried out using different soil textures and root distributions in order to evaluate the interplay between soil hydrodynamics and plant characteristics, and the impact of assuming time-constant plant physiological properties. Results show a good agreement between simulated and observed transpiration fluxes for both RWU models, with a more distinct response under water stress conditions and with uncertainty in the soil parameterization prevailing to the differences due to changes in the model formulation. The hydraulic RWU model exhibits also a lower sensitivity to the root distributions when simulating the onset of the water stress period. Finally, an analysis of variability across the soil and root scenarios indicates that differences in soil water content are mainly influenced by the root distribution, while the transpiration flux in both RWU models is additionally determined by the soil characteristics.

Highlights:

- A novel root water uptake scheme based on the hydraulic architecture approach is integrated in a terrestrial systems modeling platform.
- Root hydraulic properties control plant transpiration during prolonged dry conditions.
- Soil parameterization uncertainty strongly influences the simulation of transpiration fluxes and soil water content in different RWU models.
- Soil parameterization and roots distribution induce larger variability in the hydraulic model response compared to the standard RWU formulation.

Keywords:

root water uptake, hydraulic architecture model, hydraulic redistribution, transpiration, crop water stress, stomata conductance, minirhizotron facility, terrestrial systems modeling

1 Introduction

The understanding of plant response to water limitation is of paramount importance to improve quantification of the key component (i.e., transpiration) of the terrestrial water balance [Schlesinger and Jasechko, 2014], estimating the severity of droughts and heatwaves through land–atmosphere interactions [Teuling et al., 2010; Konings et al., 2011; Kala et al., 2016], quantifying carbon uptake of terrestrial ecosystems [Friedlingstein et al., 2006; Liu et al., 2017], and for predicting crop yield and productivity [Lobell et al., 2014]. The societal relevance of this scientific topic is expected to increase under global warming due to the increase of climate extremes [Parmesan and Yohe, 2006; Diffenbaugh and Field, 2013] and higher demands for food [Foley et al., 2011; Steffen et al., 2015].

Physical mechanisms involved in the description of soil-plant-atmosphere interactions include the water uptake/release by roots, the regulation by stomata, as well as the coordination between above- and below-ground processes through the plant vascular network. A comprehensive review on the modeling of water transport mechanisms within plant is presented in Fatichi et al. [2016] with some of the key elements briefly summarized here. Overall, in order to prevent leaves from desiccation during carbon dioxide capture from the atmosphere through stomata, plants develop dedicated mechanisms and structures. While stomata open in response to light and decreasing carbon dioxide concentration in leaf interstitial spaces, a lowered water potential of the evaporating mesophyll cell walls may in turn reduce stomatal aperture [Ripullone et al., 2007; Damour et al., 2010] in order to protect both leaves and subtending xylem tissue from dramatic cavitation [McDowell et al., 2008]. A negative water potential of mesophyll cell walls also drives suction and activates a complex water supply system, reaching down to the soil water along a network of xylem conduits and across roots [Steudle and Peterson, 1998;

Caldeira et al, 2014]. While water flows against gravity from high water potentials in the soil towards lower potentials in the leaves, the supply rate is limited by the network hydraulic properties [Sperry et al., 2002; Couvreur et al., 2014]. An increase in root hydraulic conductance increases the plasticity of water uptake locations when soil moisture is unevenly distributed [Meunier et al., 2017b; Cai et al., 2017] as well as the supply rate under water deficit. Through their impact on leaf water supply and potential, root hydraulic properties may regulate the plant water budget under water limitation [Schoppach et al., 2014; Jerszurki et al., 2017].

Sophisticated modeling approaches that resolve the stomatal function at the cellular level with the description and quantification of water fluxes across the soil-plant-atmosphere continuum have been developed in the last decades [e.g., Williams et al., 1998; Sperry et al., 1998; Porporato et al., 2001; Tuzet et al., 2003; Daly et al., 2004; Bohrer et al., 2005; Deckmym et al. 2008; Drewry et al., 2010; Manzoni et al., 2014]. The level of complexity of these models includes vertically resolved vegetation structure that accounts for gradients within the canopy space as well as the links between stomatal response to leaf water potential and its connection and coordination with plant hydraulic traits. While more complete mechanistic understanding of plant function has started to be integrated in Earth System Models (ESMs) [e.g., Bonan et al., 2014; Bouda and Saiers, 2017], several LSMs - the terrestrial components of ESMs - simulate plant transpiration with a combined stomatal conductance and photosynthesis model [e.g., Bonan, 1995; Sellers et al., 1996] using various empirical functions to describe the effect of soil moisture deficit. This effect is usually simulated via a soil status-dependent so-called beta factor by imposing either a limitation by reducing the slope of stomatal conductance-photosynthesis relationship (diffusive limitation), or a limitation by reducing the maximum carboxylation rate (Vc_{max}, biochemical limitation), or both diffusive and biochemical limitation. However, little observational evidence exists for such a functional dependence of stomata

conductance on soil moisture, which has stimulated continuous research [Zhou et al., 2013]. Egea et al. [2011] explored the impact of incorporating different soil water stress formulations in the functional relationship between stomatal conductance and photosynthesis. Similarly, Verhoef and Egea [2014] investigated the replacement of the water stress factor with equations that use soil water potential or with a set of equations that involve hydraulic and chemical signaling. Combe et al. [2016] performed numerical sensitivity experiments to evaluate the impact of different water stress formulations on the strength of land-atmosphere coupling. This work indicates that the underlying vegetation water stress response clearly impacts diurnal atmospheric processes and the response to atmospheric warming. Moreover, as an alternative to the empirical stomatal conductance model, formulations based on optimization theory have been recently introduced in LSMs. Based on the work of Williams et al. [1998], Bonan et al. [2014] proposed a stomatal conductance model that optimizes photosynthetic carbon gain per unit water loss while contrasting stomatal opening to prevent leaf desiccation. A systematic comparison against flux tower measurements showed that this model outperforms the current approach implemented in land surface models especially under water stress conditions. Similarly, De Kauwe et al. [2015a] replaced the empirical stomatal conductance model of the Australian LSM, Community Atmosphere Biosphere Land Exchange (CABLE), with a formulation based on optimisation theory which maximizes carbon gain while minimizing water losses as proposed by Medlyn et al. [2011]. Global-scale simulations performed with the new model drastically reduced transpiration fluxes for certain plant functional types, however, without noticeable reductions of known systematic model errors. Consequently, a more detailed description of stomatal closure and hydraulic traits in LSMs is required in order to improve their ability to predict ecosystem drought response, as was also suggested by recent observational evidence [e.g., Konings et al., 2017] and numerical model analysis [e.g., De Kauwe et al. 2015b].

The active role of roots in redistributing the water within the soil profile, known as root hydraulic redistribution (HR), has been investigated in a wide range of experimental [e.g., Richards and Caldwell, 1987; Burgess et al., 1998; Schulze et al., 1998; Domec et al., 2010] and numerical studies [e.g., Ryel et al., 2002; Quijano et al., 2012; Quijano et al., 2013; Quijano and Kumar, 2015] for different plant species and across a variety of climate regimes. Accordingly, in recognition of the potential role of HR on atmospheric processes [e.g., Lee et al. 2005; Siqueira et al. 2008] and on carbon and nutrient cycling [Snyder et al., 2008; Aanderud and Richards, 2009], different formulations of HR have been included in LSMs. For instance, Zheng and Wang [2007] modified the soil water flux formulation in two LSMs, namely the Community Land Model version 3 (CLM3) and the Integrated Biosphere Simulator version 2 (IBIS2), by adding the HR term as proposed by Ryel et al. [2002]. Comparisons with observed latent heat fluxes at the Reserva Biológica do Jaru site in Amazonia led to overall improved performances by both LSMs. Li et al. [2012] showed that incorporating a HR function in CABLE significantly improves the agreement between simulated net ecosystem exchange, latent heat flux, and soil moisture dynamics with observations during dry seasons. The HR parameterization developed in Ryel et al. [2002] was included in CLM4.0 by Yan and Dickinson [2014] and their comparison with measurements at nine sites in Amazonia demonstrated that vegetation and biomass response to droughts is better captured when considering the HR process. Tang et al. [2015] tested the sequentially coupled implementation of the Amenu-Kumar HR model [Amenu and Kumar, 2008] in CLM4.5 with global-scale simulations. Comparisons with eddy covariance measurements at a forested site in California showed a better representation of the seasonal evapotranspiration cycle when accounting for HR; no improvements were, however, found for another site in Amazonia. The same study advocated for a tightly coupled approach under high HR rates to achieve numerically accurate solutions. Fu et al. [2016] analysed the effect of incorporating the Ryel scheme in CLM4.5 across different ecosystems within the AmeriFlux monitoring network; their findings indicate that HR tends to more pronounced effects under strong seasonality and

for rather dense vegetation. Zhu et al. [2017] showed that incorporating HR and compensatory water uptake functions in the Common Land Model significantly reduce biases in the land surface energy partitioning over sites that experience seasonal droughts. Finally, the schemes of Ryel and Amenu-Kumar as implemented in CLM4.5 were used in Fu et al. [2018] to demonstrate the impact of HR in reducing N_2O emissions at sites characterized by a distinct dry season. While the aforementioned studies revealed the ecohydrological and biogeochemical significance of HR, the quantification of its magnitude is still characterized by large uncertainty, with nearly two orders of magnitude differences within a range of selected experimental and modeling studies conducted across different ecosystems [Neumann and Cardon, 2012]. Moreover, Schymanski et al. [2008] demonstrated that the magnitude of HR significantly decreases by relaxing the assumption of a static root profile, which is commonly implemented in LSMs. Other studies reported on the differences in the magnitude of the HR process when using different soil retention curves [Hultine et al., 2003; Prieto et al. 2010], with coarse-textured soils being less conducive to HR. Therefore, the understanding and assessment of the HR process for cropland as well as its interplay with plant physiological and soil properties require further investigations, which could potentially shed light on the large uncertainty in the quantification of agriculture-climate interactions in ESMs [McDermid et al. 2017].

This work presents the integration of a macroscopic root water uptake, hereafter RWU, model [Couvreur et al., 2012] based on the hydraulic architecture approach in the land surface component (CLM4.0, [Oleson et al., 2010]) of the Terrestrial Systems Modeling Platform, TerrSysMP [Shrestha et al., 2014]. The model uses three parameters derived from first principles: the compensatory RWU conductance determines the ability of the root system to adapt its uptake in response to the soil water distribution, while the root system equivalent conductance and the leaf water potential at stomatal closure control the transpiration response

188 to soil water limitation. The model accounts for both root density dynamics and hydraulic
189 compensatory effects (including the HR) by reformulating the water stress formulation in CLM.
190 Therefore, leveraging the detailed mechanistic understanding of individual plant models into a
191 macroscopic formulation, the proposed approach reconciles with previous and ongoing efforts
192 that seek to better connect the calculation of transpiration with root functional and structural
193 traits in LSMs [Warren et al., 2015]. Results of the standard and the new approach are
194 compared for point-scale simulations for winter wheat cultivated in a sheltered plot of the
195 minirhizotron facility in Selhausen, Germany [Cai et al., 2016] and are validated against
196 transpiration fluxes estimated from sap flow sensors and soil moisture measurements at
197 different soil depths. In order to evaluate the interplay between soil hydrodynamics and plant
198 characteristics, sensitivity experiments are carried out with different soil characterizations (e.g.,
199 soil saturated conductivity) and plant physiological properties (e.g., root distributions and root
200 hydraulic conductance).

201

202 Section 2 of this paper describes the observations, the integration of the new RWU model in
203 TerrSysMP, and the setup of scenarios based on estimates of root density distributions and
204 crop hydraulic properties. Results of the standard and new approach are compared with
205 observations in Section 3. Section 4 discusses approaches for upscaling the proposed RWU
206 scheme from the field to the global scale and for different plant functional types while Section 5
207 provides conclusions and an outlook of the work.

2 Data and methods

2.1. Minirhizotron facility: Field plot and data

The experimental setup used in this study is the upslope sheltered plot of the minirhizotron facility in Selhausen, Germany (50°52'N, 6°27'N, 103 m asl, Figure 1, Cai et al. [2016]). The plot, which is part of the TERENO observatory [Zacharias et al. 2011], is characterized by a silty soil with approximately 60% gravel. Sand and clay percentages of the fine soil in the topsoil (0-30 cm) and subsoil (30-120 cm) are 35 and 13, and 37 and 16, respectively.

Winter wheat (*Ambello* variety) was sown on 31 October 2013 and harvested on 17 July 2014. The phenological development of the crop was monitored using a plant canopy analyser (LAI-2200, LI-COR, Inc. USA), according to which the leaf area index (LAI) ranged up to 2.5. The root distributions were measured by installing a digital camera inside acrylic glass rhizotron tubes, that were placed at depths of 10, 20, 40, 60, 80, and 120 cm (Figure 1). Camera images taken at weekly intervals (22 sampling points) were analysed using the Rootfly software [Wells and Birchfield, 2009], which provide the root length and counts per image. A detailed description of the complete post-processing procedure - including inherent assumptions - for the estimation of the normalized root distribution along the soil column (Figure 2) can be found in Cai et al. [2017, 2018].

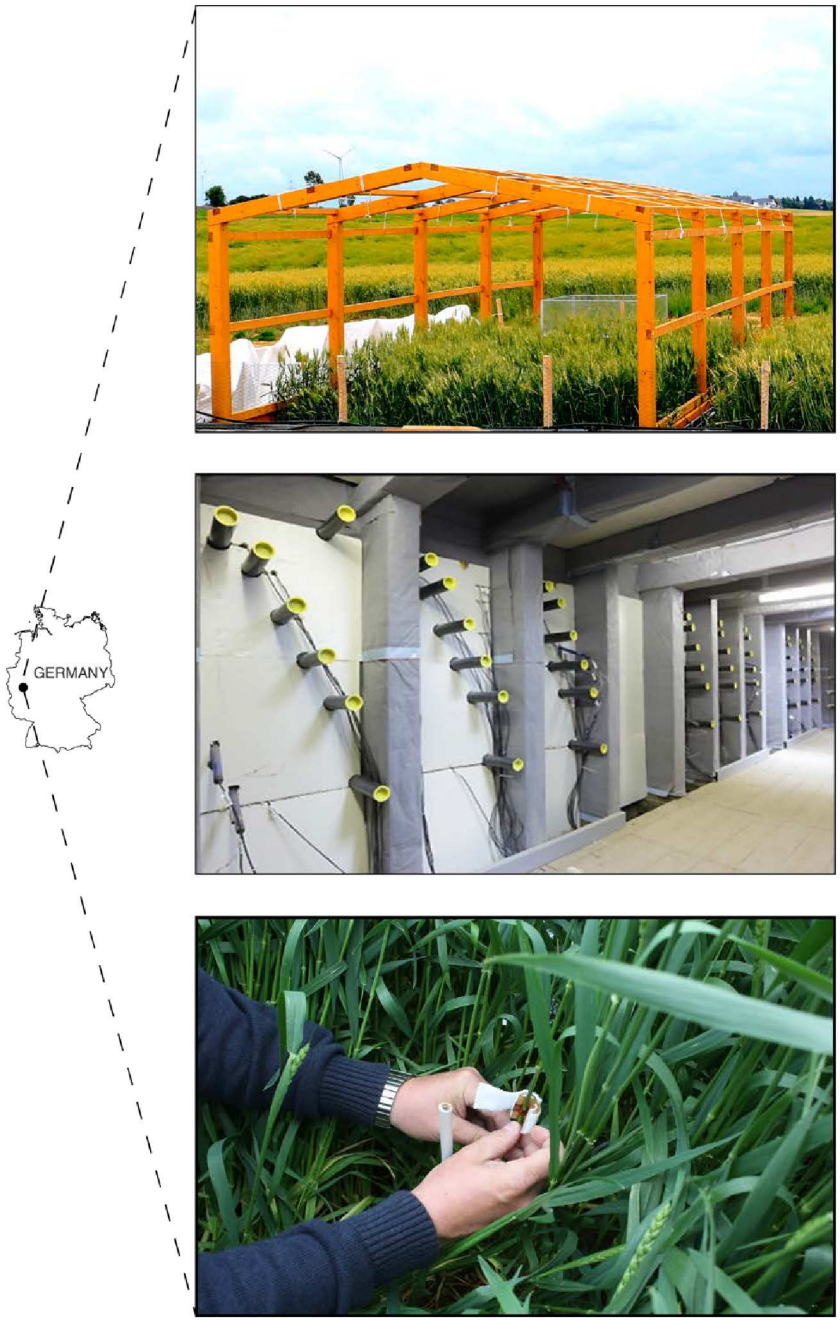

Figure 1: (Top) External view of the minirhizotron facility located in Selhausen (Germany). (Middle) Internal view of the facility with the installation of rhizotron tubes at different depths. (Bottom) Example of the sap flow sensors used to estimate the transpiration fluxes.

Winter wheat transpiration was estimated using SGA3 Dynagage sap flow sensors (Dynamax Inc., Houston, USA) installed on five wheat tillers located in the center of the plot. Temperature signals from these sensors were taken every 60 seconds with Dynamax control units consisting of voltage regulators, AM 16/32B multiplexers and CR1000 data loggers (Dynamax Inc., Houston, USA; Campbell Scientific, Logan, Utah), and post-processed to remove the noise as described in Langensiepen et al. [2014]. The area-averaged transpiration flux (mm d^{-1}) was determined by multiplying the sap flow rate (g d^{-1} $tiller^{-1}$) with the tiller density per unit area of the plot (i.e., 228 tillers m^{-2}). Note that the sensors started operating on 23 May 2014 when an adequate stem diameter for their proper installation was reached, and were removed eleven days before the harvesting day (6 July 2014).

Soil moisture was measured by time-domain reflectometry (TDR) sensors installed at the same soil depths used for the monitoring of the root development (i.e., 10, 20, 40, 60, 80, and 120 cm). Data were recorded hourly by a data logger (Model CR3000, Campbell Scientific) with multiplexer peripherals (50C81-SDM). Topp's equation [Topp et al., 1980] was used to calculate the water content from the TDR-measured dielectric permittivity of the soil. A detailed description of the procedure, including statistical tests to detect possible outliers, can be found in Cai et al., [2016].

2.2. Model formulation

The macroscopic RWU model based on the hydraulic architecture approach, hereafter HRWU, developed by Couvreur et al. [2012] was integrated in CLM4.0 [Oleson et al. 2010], which is also the land surface component of the Terrestrial Systems Modeling Platform, TerrSysMP [Shrestha et al., 2014] developed within the framework of the Transregional Collaborative Research Center 32 on "Patterns in Soil, Vegetation Atmosphere Systems" [Simmer et al., 2014].

In the standard formulation of CLM, hereafter CTRL, the RWU Q_{rwu} [LT^{-1}] for each soil layer *i* (numbered from 1 to n) is calculated according to the following equation:

$$Q_{rwu}(i) = T_{act} \cdot \frac{r_{fr}(i) \cdot r_{res}(i)}{\beta_{CTRL}} \qquad i = 1, \ldots, n \qquad (1)$$

where T_{act} [LT^{-1}] is the plant functional type (PFT) specific actual transpiration, $r_{fr}(i)$ [-] is the root fraction of the *i-th* soil layer calculated using a PFT-dependent two-parameter exponential function, $r_{res}(i)$ [-] is the root resistance, and β_{ctrl} [-] is the integral soil water availability (i.e., soil moisture limiting factor), which is used to normalized root resistances to one. The root resistance factor at each soil layer is calculated as a linear function of the soil water potential, $\psi_{swp}(i)$ [L]:

$$r_{res}(i) = max\left(0; min\left(1; \frac{\psi_{swp}(i) - \psi_{close}^{soil}}{\psi_{open}^{soil} - \psi_{close}^{soil}}\right)\right) \qquad i = 1, \ldots, n \qquad (2)$$

where the soil water potential at which stomata is fully open (ψ_{open}^{soil} [L]) and fully close (ψ_{close}^{soil} [L]) are predefined PFT-dependent parameters. The soil moisture limiting factor β_{CTRL} is

calculated as a weighted layer average of the root resistance factor with weights given by the root fraction in each soil layer:

$$\beta_{CTRL} = \sum_{i=1}^{n} r_{fr}(i) \cdot r_{res}(i) \qquad i = 1, \ldots, n \qquad (3)$$

The soil moisture limiting factor ranges between 1 and near zero; it is applied in the calculation of the maximum carboxylation rate, $V_{c_{max}}$, in order to take into account the effect of water stress on plant transpiration and photosynthesis.

In the novel HRWU scheme, the water uptake flux in each soil layer is calculated according to the following equation:

$$Q(i) = Q_{std}(i) + Q_{comp}(i) \qquad i = 1, \ldots, n \qquad (4)$$

where Q_{std} [LT^{-1}] is the distributed RWU resulting from a uniform water potential in the root zone and Q_{comp} [LT^{-1}] is the compensatory term (i.e. a plastic response of the root water uptake to the vertical soil water distribution, i.e. its sum over all layers is zero). In the HRWU scheme Q_{std} is calculated as the product of the plant functional type-specific actual transpiration T_{act} and a partitioning term:

$$Q_{std}(i) = T_{act} \cdot SSF(i) \qquad i = 1, \ldots, n \qquad (5)$$

where SSF [-] is the standard sink fraction in the *i-th* soil layer, which is here assumed to be equal to the normalized root distribution r_{fr} which sums up to 1 when integrated across all soil layers. The compensatory term in Equation (4) is calculated as follows:

$$Q_{comp}(i) = K_{comp} \cdot SSF(i) \cdot (\psi_{swp}(i) - \psi_{eq}) \qquad i = 1, \ldots, n \qquad (6)$$

where K_{comp} [$LL^{-1}T^{-1}$] is the compensatory conductance per unit horizontal area (note that water potentials are expressed in terms of water heads or water column heights), and ψ_{eq} [L] is the equivalent or average soil water potential sensed by the plant:

294

295 $$\psi_{eq} = \sum_{i=1}^{n} SSF(i) \cdot \psi_{swp}(i) \quad (7)$$

296

297 According to Equation (6) and Equation (7), Q_{comp} represents the ability of the root system to
298 adapt its uptake in response to non-uniform distribution of soil water potential describing
299 mechanistically both of the processes of RWU adjustment [Feddes and Rijtema, 1972; Doussan
300 et al., 2006] and hydraulic redistribution [Neumann and Cardon, 20102; Meunier et al., 2017b].
301 That is, a positive value of $\mathrm{Q_{comp}}$ indicates that the uptake rate at soil layer *i* is increased as
302 compared to the case of uniform soil water potential distribution while a negative value implies
303 its reduction. In this formulation, the HR process is an extreme case of compensatory RWU
304 occurring when the negative $\mathrm{Q_{comp}}$ term exceeds the atmospheric water demand scaled by the
305 root fraction. Under such reverse flow conditions the release of water from the roots is assumed
306 to be controlled by the same resistance as the water uptake process, which is a hypothesis that
307 needs to be validated by further experimental investigations. Moreover, as compared to other
308 parameterizations commonly implemented in LSMs, i.e., the model of Ryel et al. [2002], the
309 proposed formulation does not need a day-night switch to regulate the HR process, and the soil-
310 root conductance, i.e. K_{comp}, is not scaled with the soil water potential via empirical
311 relationships. Despite not explicitly solving for a coupled soil-root transport equation system, like
312 in the Amenu-Kumar approach, the macroscopic parameters of the model implicitly account for
313 the hydraulic architecture of the root system, because they are deduced from solutions of water
314 flow in a hydraulic architecture [Couvreur et al. 2012].

315

316 The actual transpiration flux T_{act} is by definition lower (by a ratio β_{HRWU} [-]) or equal to T_{pot} [L T^{-1}],
317 which is the transpiration flux obtained following the current approach of CLM based on the

Monin-Obukhov similarity theory and assuming no soil water limitation. In the proposed HRWU scheme, the water stress factor is now calculated as the ratio of water supply to potential transpiration:

$$\beta_{HRWU} = max\left(0; min\left(1; \frac{Krs \cdot (\psi_{eq} - \psi_{close}^{leaf})}{T_{pot}}\right)\right) \quad (8)$$

where K_{rs} [L L^{-1} T^{-1}] is the root system equivalent conductance, which is proportional to the leaf water supply. ψ_{close}^{leaf} [L] is the leaf water potential at stomatal closure, and T_{pot} [LT^{-1}] is the potential transpiration flux assuming no soil water limitation. As implemented in other LSMs [e.g., Egea et al., 2011], the stress factor constrains the transpiration flux via the stomatal resistance and, hence, is not anymore indirectly applied to the maximum carboxylation rate, $V_{c_{max}}$ as done in the CTRL configuration of CLM. The underlying hypothesis of the HRWU approach summarized in Equation (8) is that a hydraulic regulation depending on the water potential in the leaves (or in the root collar) is applied to the atmospheric water demand (i.e., $\mathrm{T_{pot}}$). This regulation is exerted by a resistance described via a step function that keeps the stomata opened when plant water potential is above a critical threshold (i.e., $\psi_{\mathrm{close}}^{\mathrm{leaf}}$), and regulates the transpiration flux so that the leaf water stays equal to $\psi_{\mathrm{close}}^{\mathrm{leaf}}$, as observed in near-isohydric plants [Klein, 2014]. This step function is an approximation of a non-linear response of the plant to water stress conditions, which can be represented more precisely by including an additional resistance term that is a non-linear function of the leaf water potential [Tardieu and Davies, 1993] or using a non-linear plant vulnerability curve [Sperry et al., 1998]. Moreover, in the current formulation the $\mathrm{K_{rs}}$ parameter does not account for the effect of the soil hydraulic resistance. This simplification removes, therefore, the dependence of the upscaled root system conductance to the soil water potential and soil hydraulic conductivity, as opposed to other formulations that maintain the nonlinear relationship between the bulk root system conductance parameter and the soil conditions [e.g., Sperry et al., 1998; Daly et al., 2004; Manzoni et al.,

342 2014, among others]. Analytical formulations of the soil resistance as a function of the root
343 density, the root radial resistance, and the bulk soil matric potential were derived by Schroder et
344 al. [2009] and Meunier et al., [2017b]. Overall, including the soil resistance will lead to
345 differences in the compensatory term as well as in the standard sink fraction and will reduce the
346 uptake and the exudation of water from and into drier soil layers (and reduce HR). Further
347 evaluation of the influence of the soil-root hydraulic resistance on the uptake at the root system
348 scale and how it should be implemented in an upscaled model needs further testing. Finally, the
349 current formulation of the model does not account for non-hydraulic strategies (i.e., chemical
350 signaling) that plants develop to regulate transpiration [Huber et al. 2014, Tardieu et al., 2015].

351

352 According to the equations above the HRWU scheme introduces three new plant-specific
353 parameters (i.e., K_{comp}, K_{rs}, and ψ_{close}^{leaf}), which are included in a lookup table describing the
354 physiological crop properties. These parameters (i.e., K_{comp} and K_{rs}) intrinsically account for
355 changes in the root density when prescribed according to the phenological development of the
356 plant and can be generalized as a single parameter when the root axial resistance is much
357 lower than the radial component, which also simplifies the parameterization of the model. These
358 macroscopic parameters can be predicted from measurable local structural and functional root
359 properties. For instance, Meunier et al. [2017a; 2017c; 2017d] provided mathematical functions
360 to estimate the global root conductance (i.e., $\mathrm{K_{rs}}$) from architectural ("structural") traits such as
361 root length and the distance between laterals, and hydraulic ("functional") traits such as the
362 profiles of axial and radial conductivities along roots.

2.3. Numerical experiments

Point-scale numerical simulations were performed with CLM standalone using both the CTRL and HRWU model. The runs were carried out from the tillering (11 February 2014) to the ripening period (14 July, 2014) using meteorological forcing (incoming shortwave radiation, air temperature, precipitation, wind speed, air pressure, and humidity) at an hourly time step observed at a neighbouring (~140 m distance) weather station. Precipitation and radiation were modified in order to take into account the shelter schedule as described in Cai et al. [2016]. The simulations were run at hourly time steps and results were stored at the same time frequency. Both CTRL and HRWU model were initialized by interpolating the soil water content measurements (at 10, 20, 40, 80, and 120 cm) to the default CLM vertical discretization. Finally, monthly LAI values estimated from the measurements described in section 2.1 and predefined crop-type static physiological properties were used for both model versions.

Soil porosity, saturated hydraulic conductivity, saturated matric potential, and Clapp-Hornberger (CH) exponent, are estimated by default using pedotransfer functions (PTFs) based on soil texture information (i.e., percentage of clay and sand); see Appendix A for further details on the complete set of equations. Different soil scenarios were constructed in order to take into account the uncertainty when using PTFs in ESMs; see Van Looy et al., [2017] for an exhaustive review on the subject. The first scenario (SOIL-SCEN1) used the measured porosity, which is consistent with the soil moisture measurements used to initialize the model. The saturated hydraulic conductivity, the saturated matric potential, and the CH parameter were computed according to the PTFs described in Appendix A, and by using the soil textural information provided in section 2.1 for two soil horizons. Measured soil porosity and saturated hydraulic conductivity was directly integrated into the models for the second scenario (SOIL-

		SOIL-SCEN1	SOIL-SCEN2	SOIL-SCEN3
θ[-]	Topsoil (0-30 cm)	0.325	0.325	0.325
	Subsoil (30-286 cm)	0.228	0.228	0.228
K_{sat} [mm/s]	Topsoil (0-30 cm)	$3.20 \cdot 10^{-3}$	$1.07 \cdot 10^{-2}$	$1.07 \cdot 10^{-2}$
	Subsoil (30-286 cm)	$3.40 \cdot 10^{-3}$	$5.83 \cdot 10^{-5}$	$5.83 \cdot 10^{-5}$
ψ_{sat} [mm]	Topsoil (0-30 cm)	263.9	263.9	229.0
	Subsoil (30-286 cm)	248.4	248.4	129.0
b [-]	Topsoil (0-30 cm)	2.930	2.930	2.45 (3.08)
	Subsoil (30-286 cm)	2.935	2.935	1.46 (0.11)

Table 1: Texture-dependent soil characteristics used in the different SOIL scenarios. θ is the porosity, K_{sat} is the saturated hydraulic conductivity, ψ_{sat} is the saturated matric potential, and b is the Clapp-Hornberger parameter. Values in brackets in SOIL-SCEN3 represent the b exponent used for the calculation of the hydraulic conductivity.

SCEN2) while the saturated matric potential and CH parameter were estimated using the PTFs. In the third soil scenario (SOIL-SCEN3) the complete set of measured soil characteristics was used in CLM. In this case, CH parameters were estimated by fitting the functional relationship of the CH model to the available soil water content and soil water potential. The values used in the three soil scenarios are summarized in Table 1.

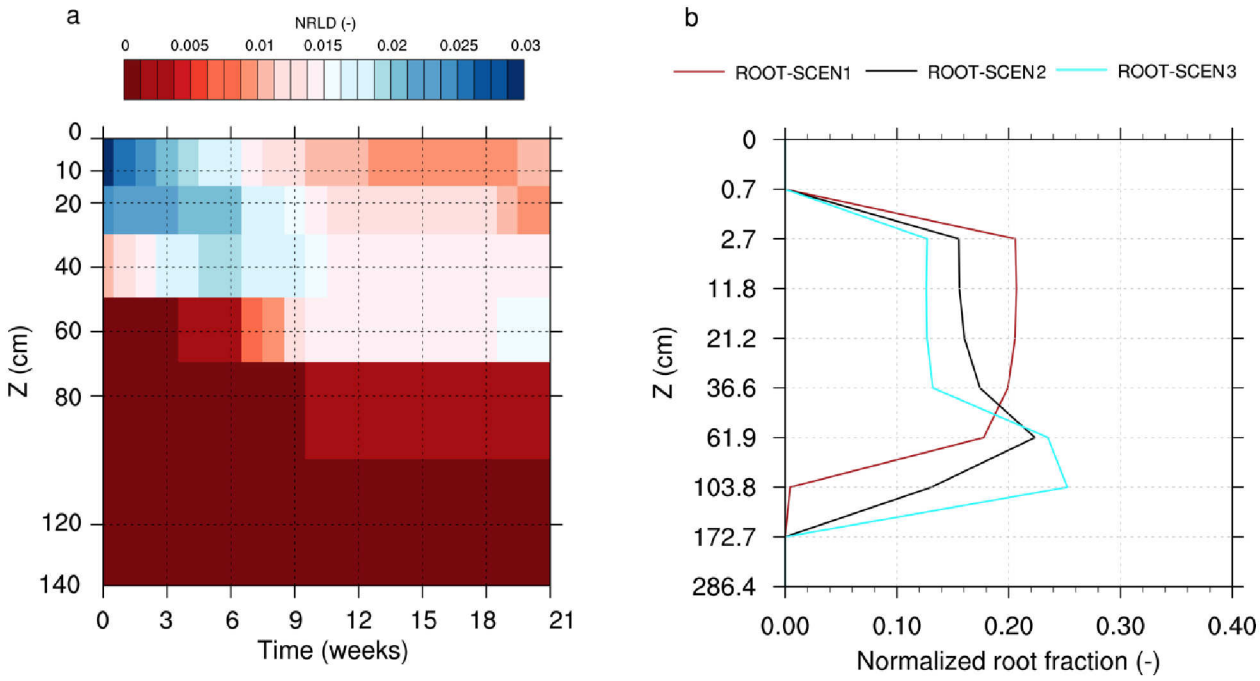

Figure 2: (a) Time evolution of the normalized root length density (NRLD) measured at different depths in the minirhizotron facility. (b) Time-static root fraction interpolated into the CLM default vertical discretization (i.e., 0.071, 2.792, 6.225, 11.886, 21.219, 36.606, 61.975, 103.802, 172.763, 286.460 cm). The three root scenarios are obtained averaging the measurements over the first five (ROOT-SCEN1), all (ROOT-SCEN2), and the last five weeks (ROOT-SCEN3) of the simulation period.

The vertical profile of the root distribution was specified by interpolating the normalized root distribution extracted by the measurements described in section 2.1, whose temporal evolution is depicted in Figure 2a, at the default vertical depths used in CLM. That is, the two-parameter exponential function used in CLM to describe the static vertical root fractions was switched off. Note also that the root fraction at the first soil layer was set equal to zero to avoid any influence of the HR process on soil evaporation, as also argued in Li et al. [2012]. By default, most LSMs assume a static representation of the vertical root distribution. In order to test the implication of such an assumption in the CTRL and HRWU model configurations, three different root scenarios were created by averaging the root distribution over different time windows of the

	HYDRA - SCEN 1	HYDRA - SCEN 2	HYDRA - SCEN 3	LEAF - SCEN 1	LEAF - SCEN 2	LEAF - SCEN 3
$K_{comp} = K_{rs}$ [m·s^{-1}·MPa^{-1}]	1.834·10^{-8}	5.036·10^{-8}	6.045·10^{-8}	5.036·10^{-8}	5.036·10^{-8}	5.036·10^{-8}
ψ_{close}^{leaf} [MPa]	-1.56	-1.56	-1.56	-2.45	-1.56	-1.07

Table 2: Crop hydraulic properties used in the HRWU model in the different HYDRA and LEAF scenarios. K_{comp} is the compensatory conductance hydraulic conductivity, assumed equal to the root hydraulic conductance (K_{rs}). ψ_{clsoe}^{leaf} is the leaf water potential at stomatal closure.

selected period (Figure 2b). That is, over the first five weeks (ROOT-SCEN1), the whole period (ROOT-SCEN2), and the last five weeks (ROOT-SCEN3) of the simulation period.

The macroscopic root hydraulic properties introduced in the HRWU model were estimated assuming the compensatory (K_{comp}) and root system (K_{rs}) conductance as equal, which was shown to be a valid assumption for relatively high root axial conductance [Couvreur et al., 2012]. As the root system architecture was not explicitly measured for the crop planted in the facility, these parameters were obtained by inverse modeling, reproducing the observed dynamics of the soil water status with a soil-plant hydraulic model (see Cai et al. [2017]). Specifically, in the inverse modeling setup of Cai et al. [2017], K_{rs} (and K_{comp}) were updated each week (obtaining 22 values over the growing season) according to the ratio of the total root length at the considered week and the root length at the week for which the initial K_{rs} was estimated using inverse modeling with a genetic algorithm. The estimated root hydraulic parameters were found to be consistent with forward calculations using literature values of root segment conductivities; see Appendix B for further information on the comparison of inverse and forward calculated K_{rs}

values. In our study, three sets of parameters were extracted from the weekly time series to mimic different root density conditions by averaging K_{rs} values over the same time windows used for the construction of the roots scenarios; namely, K_{rs} = 1.834·10^{-8} m s^{-1} MPa^{-1} for first five weeks (HYDRA-SCEN1), K_{rs} = 5.036·10^{-8} m s^{-1} MPa^{-1} for all weeks (HYDRA-SCEN2), and K_{rs} = 6.045·10^{-8} m s^{-1} MPa^{-1} for the last five weeks (HYDRA-SCEN3) of the simulation period. Finally, three scenarios were hypothesized according to plausible estimations of leaf water potential values obtained from literature review [Wesseling et al., 1991; Tardieu and Simonneau, 1998]; namely, ψ_{close}^{leaf}= -2.45 MPa (LEAF-SCEN1), ψ_{close}^{leaf} = -1.56 MPa (LEAF-SCEN2), and ψ_{close}^{leaf} = -1.07 MPa (LEAF-SCEN3). The values used in the different scenarios are summarized in Table 2.

The sensitivity experiments, which involve physiological (e.g., root distributions) and hydraulic (e.g., root system conductance and leaf water potential) crop properties were performed for each soil scenario. In doing so, SOIL-SCEN1 was selected as a reference configuration, which also closely reflects the standard implementation of LSMs. We used full-period time-averaged properties, by combining values from the ROOT-SCEN2, HYDRA-SCEN2, and LEAF-SCEN2 scenarios. The other configurations were obtained by changing one single parameter at a time, which results in total of seven additional runs per soil scenario.

3 Results and discussion

The results of the proposed HRWU model are first evaluated by comparison with sap flow measurements of transpiration fluxes and soil water content from TDR sensors installed at four different soil depths. Results of the HRWU model are also compared with the CTRL RWU scheme implemented in CLM. The model comparison and evaluation against observations are

carried out for the three soil scenarios described in Table 1. In a second step, the sensitivity of HRWU model in terms of transpiration, soil moisture, and compensatory fluxes variability, is analysed by varying the newly introduced physiological parameters within plausible value ranges found in the literature. These numerical experiments are performed using the reference model configuration (i.e., SOIL-SCEN1). The sensitivity analysis is also used to develop a mechanistic interpretation of the HRWU model response. Finally, the role of different root distributions as well as their interplay with soil characteristics is investigated for both the CTRL and the HRWU model.

3.1. Model validation and benchmarking

The performance of the two RWU models in reproducing daily transpiration fluxes and hourly soil water content at four different soil depths is summarized using Taylor diagrams [Taylor, 2001]. These plots (Figure 3) allow the simultaneous visualization of multiple statistical parameters when comparing simulations with observations on a quarter disk. The radial distance from its origin is the standard deviation of the simulated variable normalized by the standard deviation of the observations (σ_s/σ_o); the REF line (normalized standard deviation = 1) represents the variability of the observations. The azimuthal position indicates the linear correlation between the simulated and observed variables ranging from 1 (horizontal line) to 0 (vertical line). In such a plot, the REF point at r =1 and σ_s=σ_o indicates perfect agreement between observations and simulations while the radial distance from the REF point gives the normalized root-mean-square error between observations and simulations.

Figure 3a compares the transpiration from the CTRL and HRWU model simulations based on the three soil scenarios with the sap flow measurements. For the reference SOIL-SCEN1

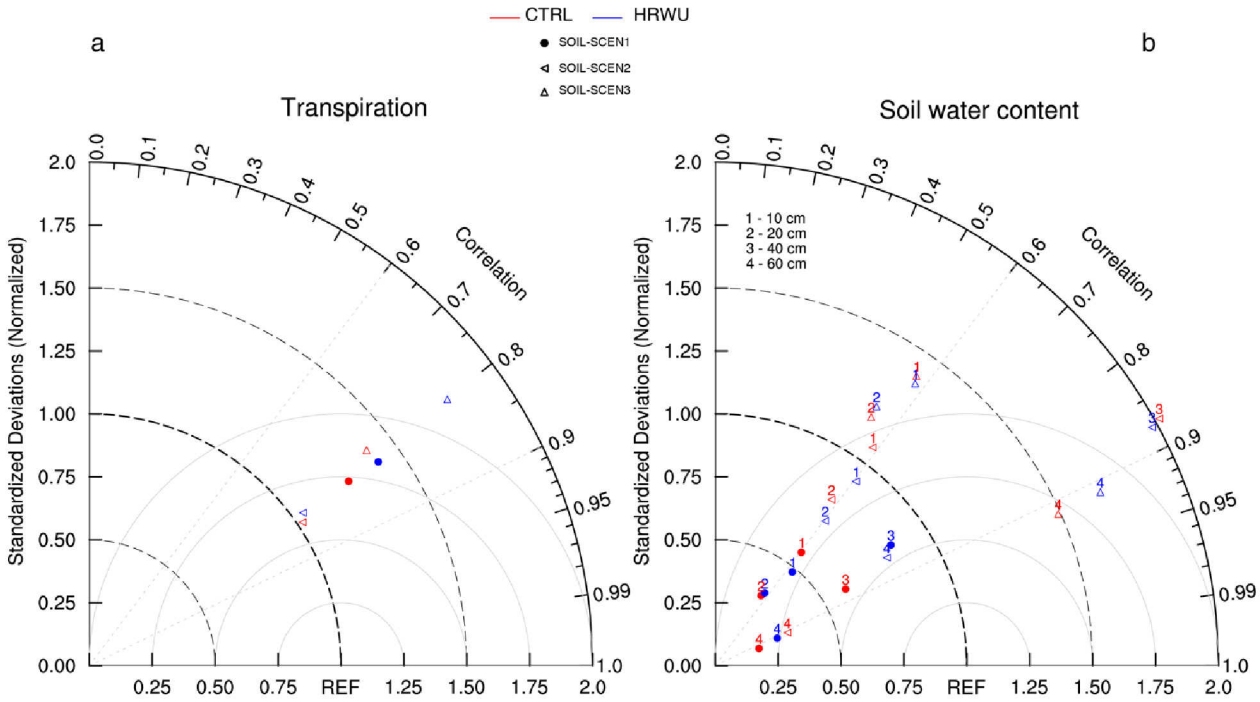

Figure 3: (a) Statistics of the simulated daily transpiration fluxes and (b) hourly soil water content interpolated at the different measurement depths for the three soil scenarios. Note that at 40 cm depth the metrics of the soil water content for SOIL-SCEN3 are outside the selected range.

scenario both models exhibit similarly good performance in terms of phase (i.e. good correlation), a similarly overestimated variability (above the REF line σ_s/σ_o = 1), and thus similar root-mean-square error with respect to the observations. The best performance of both RWU schemes is achieved for the SOIL-SCEN2 scenario, which uses for the topsoil a higher and for the subsoil a lower saturated hydraulic conductivity. The performance of the models diverges when the most detailed soil parameterization is used (SOIL-SCEN3), which also incorporates fitted parameters describing the nonlinearity of the soil retention curves. In this scenario, the HRWU scheme largely overestimates the variability of the transpiration fluxes compared to the sap flow measurements. Overall, skills increase with respect to the reference soil configuration for SOIL-SCEN2 and decrease for SOIL-SCEN3. The analysis of the models skill shows also that the results of both RWU models strongly depend on the soil characteristics. This implies

493 that changes in the summarizing statistics are remarkable when using different soil scenarios
494 and less evident when switching between the two RWU formulations.

495

496 Figure 3b shows the model performances for soil moisture. Models skills largely differ for
497 different soil depths for all soil scenarios. While soil moisture dynamics are well reproduced at
498 10- and 20-cm soil depth for the SOIL-SCEN2 scenario, performance declines for deeper soil
499 levels. Both the CTRL and HRWU model largely underestimate the amplitude of soil moisture
500 variations at 10-, 20-, and 60-cm depth for the reference soil scenario SOIL-SCEN1. It is
501 remarkable that according to the correlation coefficient, the skill of both RWU schemes using
502 the three soil scenarios aligns along two correlation lines: the results for 10 and 20 cm align with
503 r = 0.5-0.6 while the results for 40 and 60 cm align with r = 0.8-0.9. This model response can
504 be explained by a too fast recession process in the topsoil layers caused by an adjustment of
505 the soil moisture profile from the initial conditions. Overall, while minor differences were found
506 for soil water content skill statistics between the two RWU formulations, such differences are
507 notable for the different soil scenarios of the same RWU model. Larger differences between the
508 CTRL and HRWU are observed at 40- and 60-cm depth where most roots are located. The
509 estimation of soil moisture dynamics clearly improves for the new HRWU model at these
510 depths. Overall, despite a plausible performance for both RWU models in reproducing the
511 observations, a systematic mismatch between simulations and observations can be observed,
512 which persists even when including detailed soil information (i.e., SOIL-SCEN3). This suggests
513 model structural errors (e.g., free-drainage boundary condition at the soil bottom) and/or
514 unrealistic model parameterization (e.g., high stone content not taken into account) that cannot
515 be compensated by the proposed RWU scheme.

516

3.2. Sensitivity analysis

Additional insight on the relative difference between the CTRL and HRWU model response yields a sensitivity analysis by varying the two physiological parameters included in the HRWU model, namely K_{rs} (= K_{comp}) and ψ_{close}^{leaf}, as described in the scenario definition in section 2.3. The time evolution of the simulated and measured transpiration fluxes (Figure 4a) shows that the different crop hydraulic parameters play a major role. The model simulations diverge after about day 92 until the irrigation event at day 119, and again toward the end of the simulation. During most of the simulation time the transpiration is not supply-limited in the HRWU runs; under such conditions a larger K_{rs} increases the supply, which explains why the upper bound of the envelope almost coincides with the transpiration fluxes obtained using the HYDRA-SCEN2 crop hydraulic parameters (solid thick line in Figure 4a). This is also visible in the relation between the equivalent soil water potential sensed by the plant (ψ_{eq}) and the simulated transpiration for the HYDRA- scenarios (Figure 5a). That is, root hydraulic conductance values representing average or late stage growth conditions of the plant (i.e., HYDRA-SCEN2 and HYDRA-SCEN3) determine the water stress conditions under relatively similar equivalent soil water potentials, with strong water-limited conditions simulated at very negative values of soil water potentials. On the contrary, supply limited conditions are extended for relatively high soil water potentials, which may cover values relatively close to zero (i.e., relatively wet conditions), when using low root hydraulic conductance values (HYDRA-SCEN1) that mimic an early stage plant development with relative low root density. The CTRL and HRWU models respond differently to the soil drying process (Figure 4a) with the HRWU model better matching the sap flow measurement between days 105 and 118 before the irrigation event when the plants experience water stress. The contrasting response between the two RWU models corroborates, therefore, the role played by the revised water stress formulation as well as the hydraulic compensatory effect (including the HR process) in simulating crop transpiration under dry soil

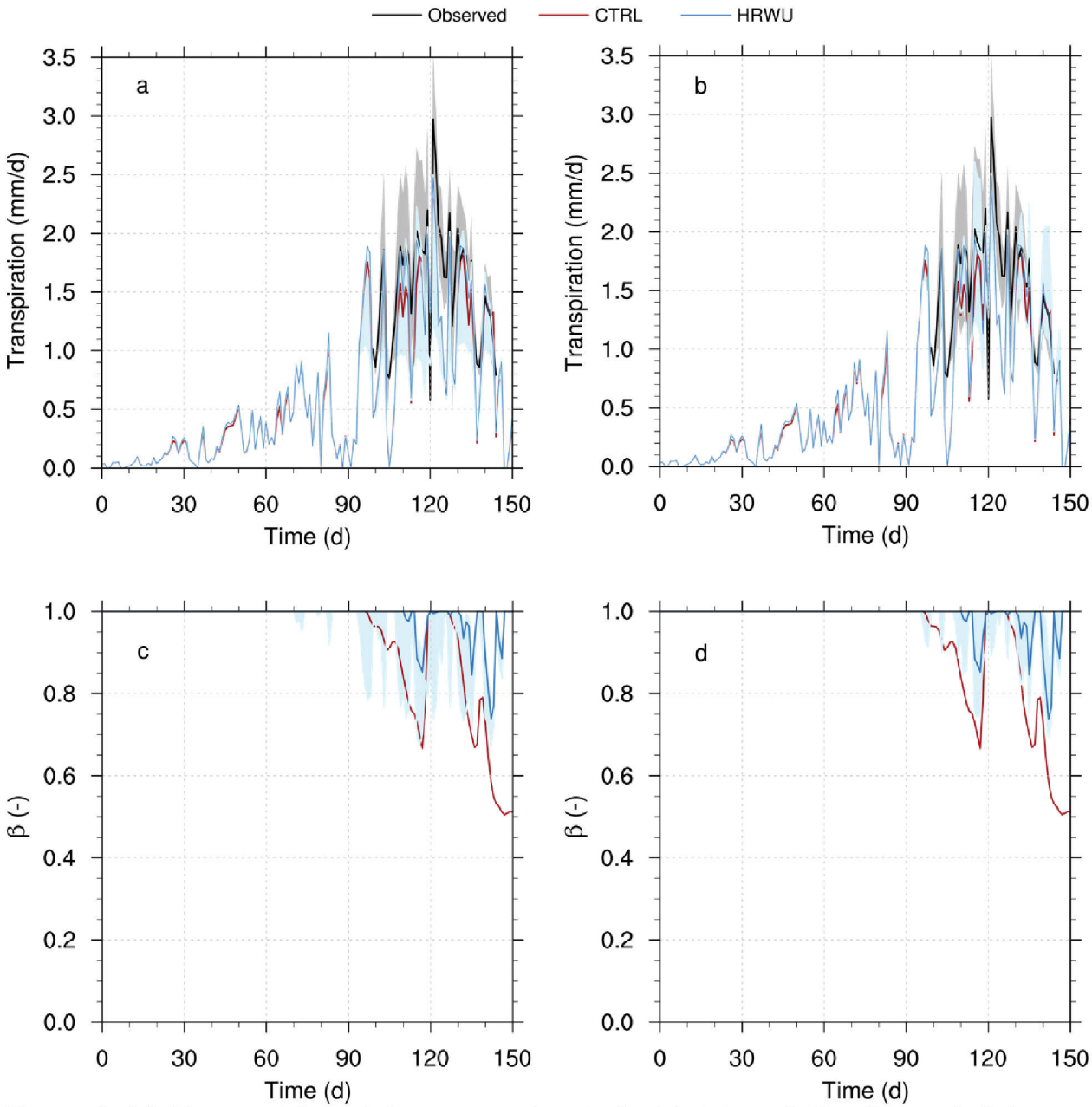

Figure 4: (a) Time evolution of the measured and simulated transpiration fluxes at Selhausen minirhizotron facility based on SOIL-SCEN1. The envelope of the HRWU model is defined by the min ($1.834 \cdot 10^{-8}$ m s^{-1} MPa^{-1}) and max ($6.045 \cdot 10^{-8}$ m s^{-1} MPa^{-1}) values of K_{rs} inverted during the simulation period. (b) Same as (a) with the envelope of the HRWU model defined by the min (-2.45 MPa) and max (-1.07 MPa) values of ψ_{close}^{leaf}. The envelope of the sap flow measurements is the variability between the five sensors. (c) Time evolution of the transpiration limiting factor (i.e., β) simulated by the CTRL and HRWU model for the HYDRA scenarios. (d) Same as (c) for the LEAF scenarios.

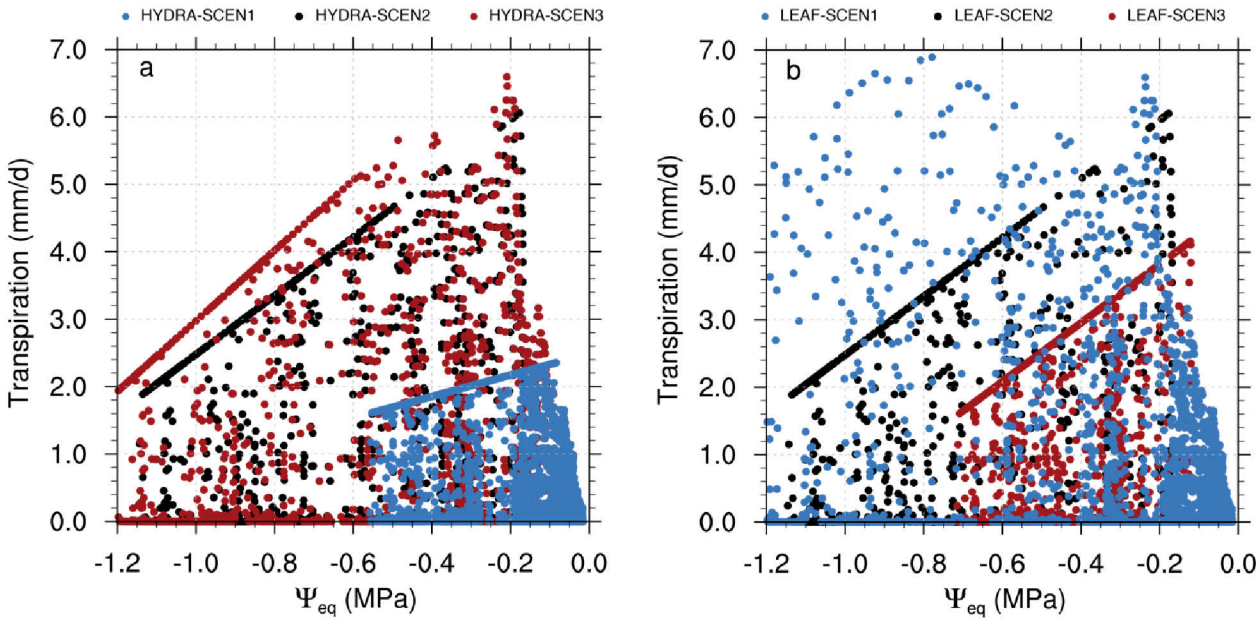

550

551 **Figure 5**: (a) Scatter plot between the equivalent soil water potential sensed by the plant (ψ_{eq}) and the
552 transpiration fluxes for the HYDRA-SCEN1 (K_{rs} = 1.834·10^{-8} m s^{-1} MPa^{-1}), HYDRA-SCEN2 (K_{rs} =
553 5.036·10^{-8} m s^{-1} MPa^{-1}), and HYDRA-SCEN3 (K_{rs} = 6.045·10^{-8} m s^{-1} MPa^{-1}) scenario. (b) Same as (a) for
554 the LEAF-SCEN1 (ψ_{close}^{leaf}= -2.45 MPa), LEAF-SCEN2 (ψ_{close}^{leaf}=-1.56 MPa), and LEAF-SCEN3 (ψ_{close}^{leaf}=-
555 1.07 MPa) scenario.

556 conditions, which has been investigated in previous studies for shrub, grasses, and trees [e.g.,
557 Caldwell et al. 1998; Oliveira et al. 2005; Domec et al. 2010; Verma et al. 2014] and more
558 recently for seasonal plant species [Soylu et al. 2017; Meunier et al. 2017b].

559

560 The sensitivity of the simulated transpiration fluxes to the use of different leaf water potential
561 values is evaluated in Figure 4b. In this case, the variability introduced by the physiological
562 property of the crop induces changes in the HRWU model response that tend to be triggered
563 later in time (~ 110 d) and to be more pronounced right before the irrigation event and towards
564 the end of the simulation period. Figure 4c and Figure 4d shows the time evolution of the
565 transpiration limiting factor (i.e., β) for both RWU model formulations and considering both the

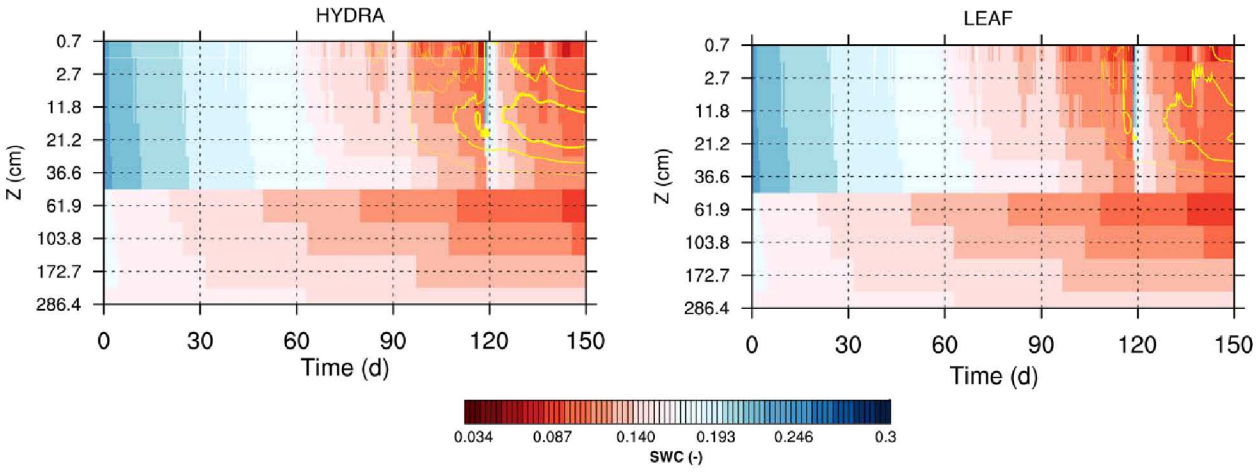

566

567 **Figure 6**: Time evolution of the simulated soil water content for the HYDRA (left) and LEAF (right)
568 scenarios of the HRWU model. Values represent the average between the scenarios described in section
569 2.3 while the yellow contour lines indicate the standard deviation. Note that the range in the contour lines
570 is between 0.002 and 0.021 with an interval of 0.005. Thicker lines indicate larger spread in the simulation
571 results.

572 HYDRA and LEAF scenarios of the HRWU model. Results confirm less supply-limited
573 conditions, especially for the HYDRA-SCEN1 and LEAF-SCEN3 scenarios, and a delayed onset
574 of the water stress conditions simulated by the HRWU model. Accordingly, between 90 and
575 150d of the simulation time period, the average water limiting factors for CTRL is $\beta_{\mathrm{CTRL}} =$
576 0.83 and $\beta_{HRWU-HYDRA-SCEN1} = 0.97$, $\beta_{\mathrm{HRWU-HYDRA-SCEN2}} = 0.96$, $\beta_{HRWU-HYDRA-SCEN3} = 0.86$
577 for the HYDRA scenarios, while $\beta_{\mathrm{HRWU-LEAF-SCEN1}} = 0.92$, $\beta_{\mathrm{HRWU-LEAF-SCEN2}} = 0.96$,
578 and $\beta_{HRWU-LEAF-SCEN3} = 0.99$ for the LEAF scenarios. Overall, the total amount of transpiration
579 during the growing season measured with the sap flow sensors (between 99 and 144d of the
580 simulation time when sap flow was measured) is 71.1±12.3 mm while the cumulative value
581 simulated with the CTRL model is 53.81 mm. Cumulative values simulated by the HRWU model
582 are 55.0±12.3 mm and 57.9±9.2 mm for the HYDRA and LEAF scenarios, respectively. These
583 bulk quantities indicate a relative difference between the two RWU approaches of about 2-7% of
584 the total transpiration measured by the sap flow sensors with about 13-17% variations among

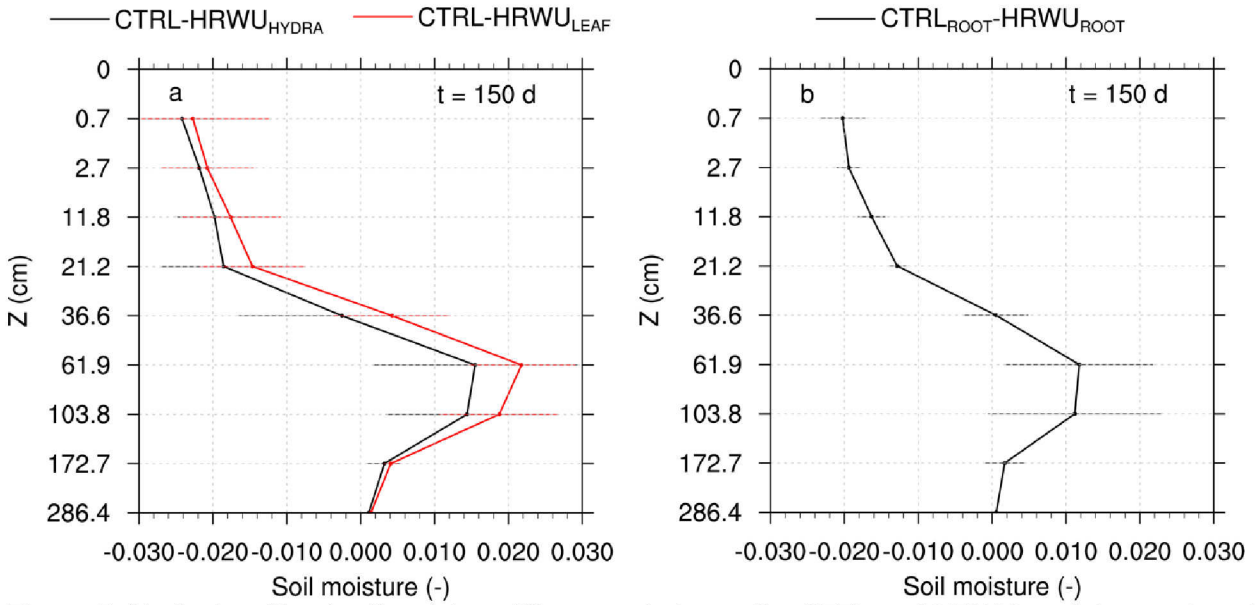

Figure 7: Vertical profile of soil moisture differences between the CTRL and HRWU model scenarios at the end of the simulation time period. Horizontal lines indicate the standard deviation of the HYDRA (a), LEAF (a), and ROOT (b) scenarios.

the different HRWU model scenarios, which reflects the non-negligible impact of the large uncertainty of its hydraulic parameterization. Finally, it is noteworthy that the spread/envelope in the sap flow measurements shown in Figure 4a and Figure 4b, which can be attributed to the variability between the five sensors, is comparable or even larger, than the one related to the variation of physiological parameters introduced in the HRWU model. Moreover, the spatial variability in the transpiration fluxes might also reflect variability in the physiological properties and/or rooting depth within the population of plants, which is not taken into account in the current HRWU model parameterization.

The relation between the equivalent soil water potential sensed by the plant (ψ_{eq}) and the simulated transpiration shown in Figure 5 for the HYDRA and LEAF scenarios provides a mechanistic interpretation of the HRWU model response. Here, it is important to recall that K_{rs} controls the slope of the water supply curve (defined by the numerator in Equation (8) and representing the transpiration as a function of the equivalent soil water potential when the leaf

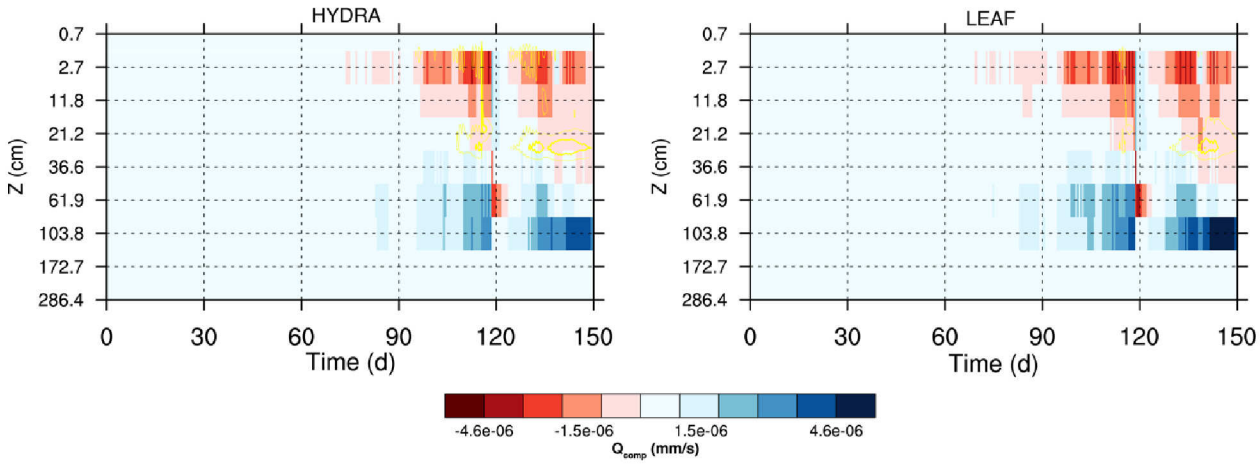

Figure 8: Time evolution of the compensatory flux for the HYDRA (left) and LEAF (right) scenarios of the HRWU model. Values represent the average Q_{comp} between the scenarios described in section 2.3 while the yellow contour lines indicate the standard deviation. Note that the range in the contour lines is between 0 and $4.0 \cdot 10^{-6}$ with an interval of $1.0 \cdot 10^{-6}$. Thicker lines indicate larger spread in the simulation results.

water potential is equal to ψ_{close}^{leaf}) while ψ_{close}^{leaf}represents the intercept of such curve with the soil water potential x-axis; see sketch in Figure 1 of Couvreur et al., [2014] for a more complete discussion. Accordingly, the possible range of soil matric potentials generating water limitation is extended up to wetter soil conditions for lower K_{rs} (e.g., due to low rooting density), though the range of soil matric potentials actually experienced by the plant in our simulation is narrower due to the reduced transpiration rates (blue dots in Figure 5a). Figure 5b illustrates that moving ψ_{close}^{leaf} toward less negative values (e.g., 0.5 MPa shift from black to red dots), translates water limitation to higher water potentials (i.e., wetter soil conditions), but the slope of the relation between supply limit and soil matric potential is conserved. The plant drought strategy mimicked by the HRWU model is, therefore, an approximation of the isohydric response where plants close their stomata rapidly maintaining a relatively high water potential along the supply limit line to lessen embolism. Recent findings reported by Martin-StPaul et al. [2017] and obtained combing a meta-analysis of plant hydraulic traits and numerical simulations demonstrate the

621 coordination between stomatal closure and the plant hydraulic capacity. That is, the stomatal
622 behaviour and the maintenance of the supply capacity of the plant hydraulic system evolve
623 along different trajectory under drought conditions. The testing of such plant functioning with the
624 HRWU model would require an upgrade of its current formulation including also a dynamic
625 calculation of the whole plant resistance according to the concept of plant vulnerability curve.

626

627 Figure 6 shows the time evolution of the average vertical profile of soil moisture for the HYDRA
628 (i.e., perturbation of the compensatory and root conductance) and LEAF (i.e., perturbation of the
629 leaf water potential) scenarios of the HRWU model. In these plots, the variability within each
630 scenario is represented by yellow contour lines. A visual inspection of the plots confirms the
631 larger sensitivity, within the ranges of specific selected values, of the HRWU model response to
632 changes in the root conductance (and compensatory) term, as also indicated by the density and
633 thickness of the contour lines for the simulation results of the HYDRA scenario. The spread in
634 the simulation results of the LEAF scenario appears just before the irrigation event and at the
635 end of the simulation period. Moreover, the overlay between the average soil moisture
636 conditions and standard deviation of each scenario shows that the variability in the model
637 response coincides also with the attainment of an 'adjusted' vertical profile of soil moisture from
638 the interpolated measured initial conditions. That is, during the first part of the simulation the soil
639 moisture hydrodynamics buffer the variability induced by the perturbation of the crop
640 physiological properties associated both to the hydraulic compensation and HR processes,
641 which compares well with findings of a previous study by Siqueira et al. [2008]. Figure 7 shows
642 the vertical profile of the soil moisture difference between CTRL and HRWU scenarios at the
643 end of the simulation time period (t = 150 d). This plot provides an integrated measure of the
644 impact of the two RWU formulations on the soil water balance, and indicates that soil moisture
645 differences (CTRL-HRWU scenarios) range between -0.0025 and -0.024 at the topsoil (0-11.8

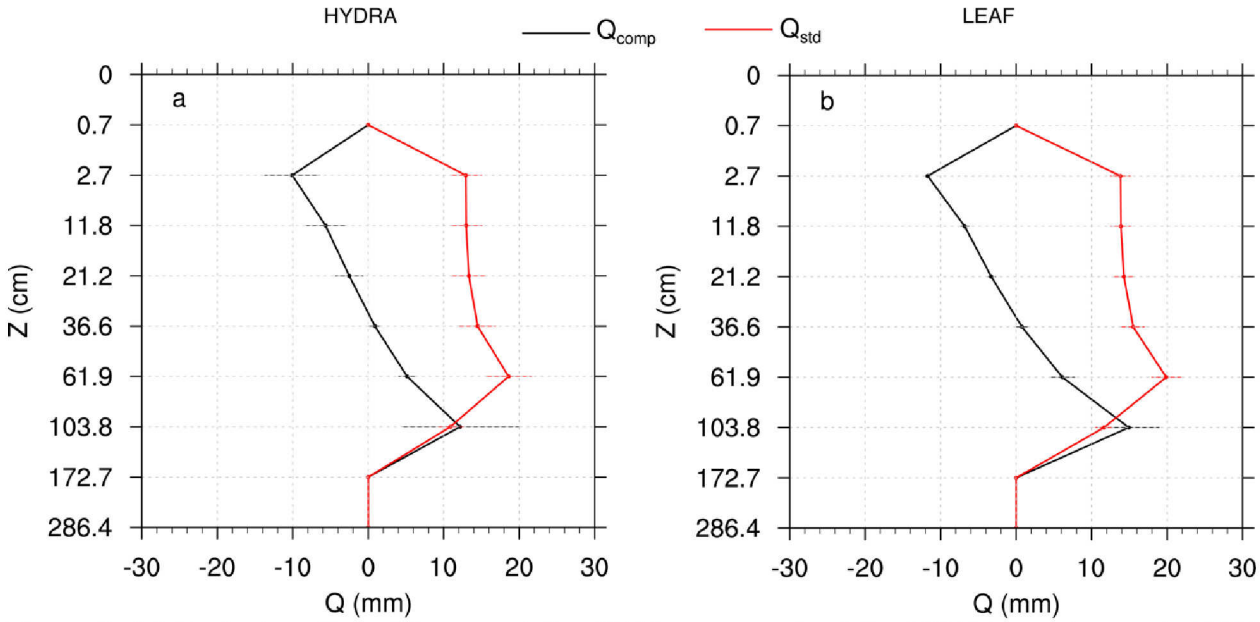

Figure 9: (a) Vertical profiles of the cumulative RWU components of the HRWU model, namely RWU under uniform soil water potentials (Q_{std}) and the compensatory RWU (Q_{comp}). Horizontal lines indicate the standard deviation of the HYDRA scenarios. (b) Same as (a) for the LEAF scenarios.

cm) and between positive 0.003 and 0.021 at the subsoil (36.6-61.9 cm) layers. This indicates that the HRWU model simulates wetter and drier soil moisture conditions at the top and bottom soil layers, respectively. Another interesting aspect found from the analysis of the vertical profiles of soil moisture differences is that changes of transpiration fluxes induced by the HYDRA scenario generate larger soil moisture variability especially between 11.8 and 103.8 cm soil depth.

Figure 8 shows the time evolution of the compensatory flux for the HYDRA and LEAF scenarios of the HRWU model, with positive values indicating an increased uptake rate at the considered soil layer as compared to the case of uniform soil water potential distribution while negative values implying its reduction. Accordingly, a larger water uptake is occurring between 61.9 and 103.8 cm soil depth for both the HYDRA and LEAF scenarios, with the latter scenario characterized by larger compensatory rates as also indicated by the analysis of the soil moisture

663 profiles differences at the end of the simulation period (Figure 7). A cross comparison of the two
664 plots indicates also the active role of the compensatory RWU process in taking up more water
665 from deep soil layers during the drying phase of the simulation and the inverse occurring for few
666 days right after the irrigation event at 119 d simulation time. Figure 9 shows the partitioning of
667 the RWU into the standard (assuming uniform water potential distributions) and the
668 compensatory component at different soil depths. According to Equation (5) and Equation (6),
669 the standard RWU component mirrors the root fraction distribution (see Figure 2) with a
670 maximum at 61.9 cm soil depth. The compensatory term peaks at 103.8 cm soil depth due to
671 the locally stronger gradient between the equivalent soil water potential sensed by the plant and
672 the soil water potential. Cumulated over the whole simulation time period, the compensatory
673 term of the HRWU sensitivity experiments varies between 14±7% at 103.8 cm and -12±2% at
674 2.7 cm soil depth of the total transpiration for the HYDRA scenarios, and between 16±3% and -
675 13±0.8% at the same soil depths for the LEAF scenarios. The magnitude of water fluxes
676 associated with HR can be quantified by screening for negative compensatory RWU fluxes that
677 are higher in absolute value than the standard uptake term. At the minirhizotron experimental
678 setup such conditions mostly occur between 2.7 cm and 11.8 cm soil depth and within a range
679 of 10±3% and 12±0.4% of the total transpiration for the HYDRA and LEAF scenarios,
680 respectively. These estimates reflect probably the special atmospheric conditions (i.e., low solar
681 radiation) due to the sheltering of the facility, which may favour the occurrence of the HR
682 process. Indeed, by screening also for nighttime conditions, when most likely the HR process
683 takes place under unsheltered conditions, its contribution drastically decreases to 4±1% and
684 5±0.3% for the HYDRA and LEAF scenarios, respectively. Overall, this numerical assessment
685 of the HR process, which is in agreement with previous numerical studies [e.g., Quijano and
686 Kumar, 2015] suggest, therefore, the importance (and the associated uncertainty) of the HR
687 process for cropland under prolonged water stress conditions.

3.3. Role of roots and soil characteristics

The sensitivity of the CTRL and HRWU model response to the different root distribution is shown in Figure 10 and Figure 11. The onset of the envelope characterizing the variability of the transpiration fluxes (Figure 10) appears slightly delayed by a few days in the HRWU model, as can be observed from a close comparison of the models response between 105 and 110 d simulation time. This could be attributed to the redistribution of the soil moisture in the shallower layers that alleviates differences between the HRWU model configurations due to the use of different root fraction scenarios. On the contrary, towards the end of the simulation, i.e. between 130 and 145 d, the HRWU model experiences a slightly larger sensitivity to the root distribution. Indeed, as the simulation advances in time, and hence the soil gets drier, deeper layers sustain the transpiration, as can be inferred from the downward shift in the soil moisture variability depicted in Figure 11. Under such conditions, the HR process takes place mostly within soil layers at 2.7-21.2 cm depth while the uptake of water increases in the deeper soil layers where contrasting root fractions characterize the ROOT scenarios, which ultimately explains the larger spread in the transpiration fluxes simulated by the HRWU model at the end of the simulation time. Figure 11 provides also a way to better identify the impact of the RWU formulations to the simulated soil moisture distribution. Specifically, according to the formulation implemented in the CTRL model, which controls the partitioning of the transpiration via a locally-defined wilting factor, as the simulation advances in time drier conditions and stronger soil moisture gradients are simulated at shallower (i.e., 0-21.2 cm) soil depths while the water content steadily and smoothly decreases at deeper layers (i.e., 61.9-103.8 cm). A different response can be observed for the HRWU model due to the simulation of the HR process and to the centralized response of total water uptake to leaf water potential (as opposed to a sum of local responses to soil water potential in the CTRL). That is, soil water content is uniformly redistributed in the first soil layers with a more pronounced decrease simulated at 61.9-103.8 cm due to the active role

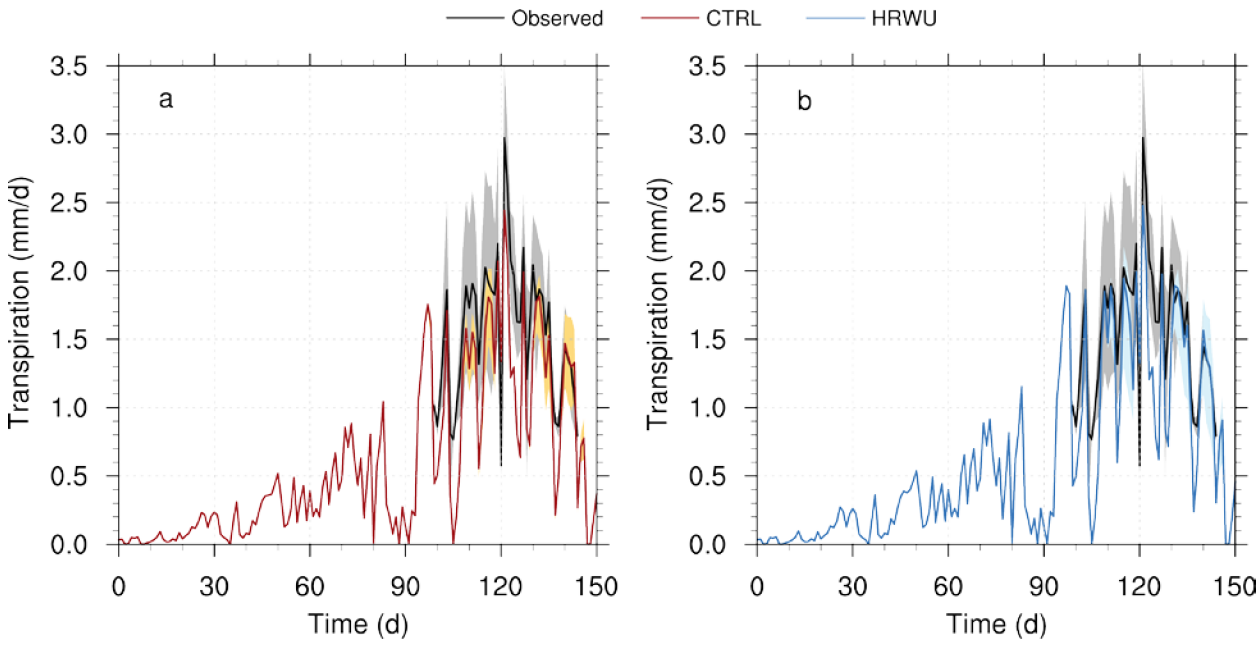

713

714 **Figure 10**: (a) Time evolution of the measured and simulated transpiration fluxes for the CTRL model at
715 Selhausen minirhizotron facility based on SOIL-SCEN1, and with the envelope defined according to three
716 root distributions depicted in Figure 2b. (b) Same as (a) for the HRWU model.

717 of roots in lifting water to upper soil layers (see Figure 8). Note also that at this depth (i.e., 40
718 cm) soil moisture variability simulated by the HRWU matches better with the observations
719 (Figure 3) for the reference soil scenario (i.e., SOIL-SCEN1). Overall, it appears that in the
720 HRWU model a larger extent of the soil vertical profile is involved for satisfying the atmospheric
721 water demand, which may contribute to better predictions of cropland drought response
722 simulated by ESMs.

723

724 The connection established between soil moisture hydrodynamics and plant hydraulic properties
725 constitutes an important piece of information that has been missing previously to evaluate
726 different RWU formulations and approaches. Figure 11 shows the role of roots distributions and
727 soil parameters in determining the transpiration fluxes for both RWU formulations. The standard
728 deviation represents the variability induced for each SOIL and ROOT scenario by changes in

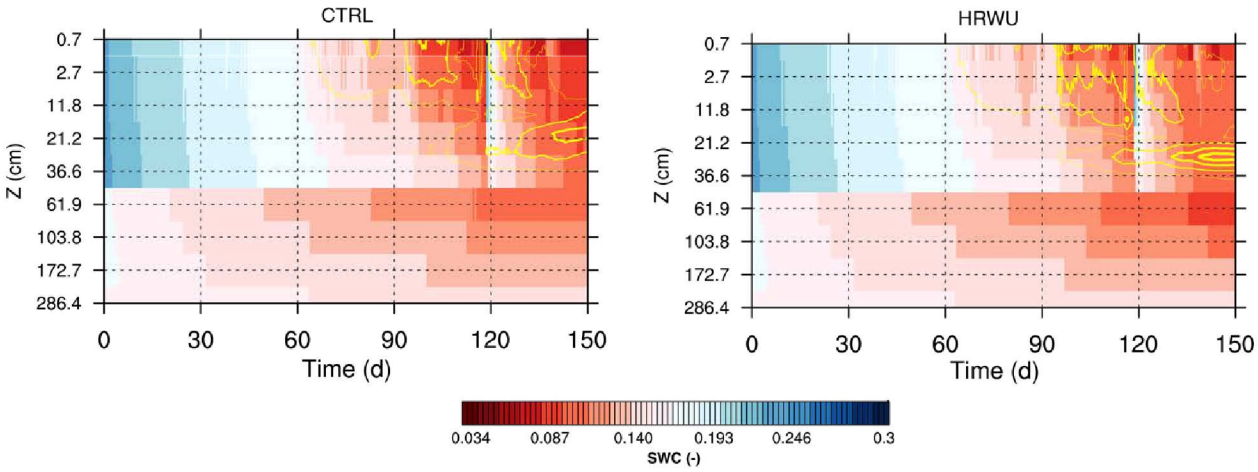

729

730 **Figure 11**: Time evolution of the simulated soil water content for the CTRL (left) and HRWU (right) model.
731 Values represent the average between the ROOT scenarios shown in Figure 2b while the yellow contour
732 lines indicate the standard deviation. Note that the range in the contour lines is between 0.002 and 0.011
733 with an interval of 0.003. Thicker lines indicate larger spread in the simulation results.

734 the vertical root fractions (Figure 12a and Figure 12b) and soil characteristics (Figure 12c and
735 Figure 12d), as described in section 2.3, respectively. Results indicate that the standard
736 deviation is generally larger for the transpiration fluxes simulated by the HRWU model. The
737 larger temporal variability of the standard deviations of simulated transpiration by the HRWU
738 model for different root distributions model also suggests a stronger interdependence between
739 soil moisture states and plant growth stages (i.e., root vertical distribution) in the regulation of
740 the transpiration flux in the hydraulic RWU formulation. Moreover, the analysis of the standard
741 deviation confirms that the variability induced by both treatments (i.e., root and soil
742 perturbations) increases when plants experience water-stress conditions (i.e., 105-119 d and
743 130-145 d) for both RWU formulations. Finally, the deviation in the transpiration fluxes for
744 different soil and root parameterizations is triggered few days later in the HRWU model
745 simulations when using SOIL-SCEN1 and SOIL-SCEN3, which coincides with a delayed onset
746 of water stress in the hydraulic RWU model. The analysis of the standard deviation for each
747 SOIL and ROOT scenario was also performed for the simulated soil water content at different

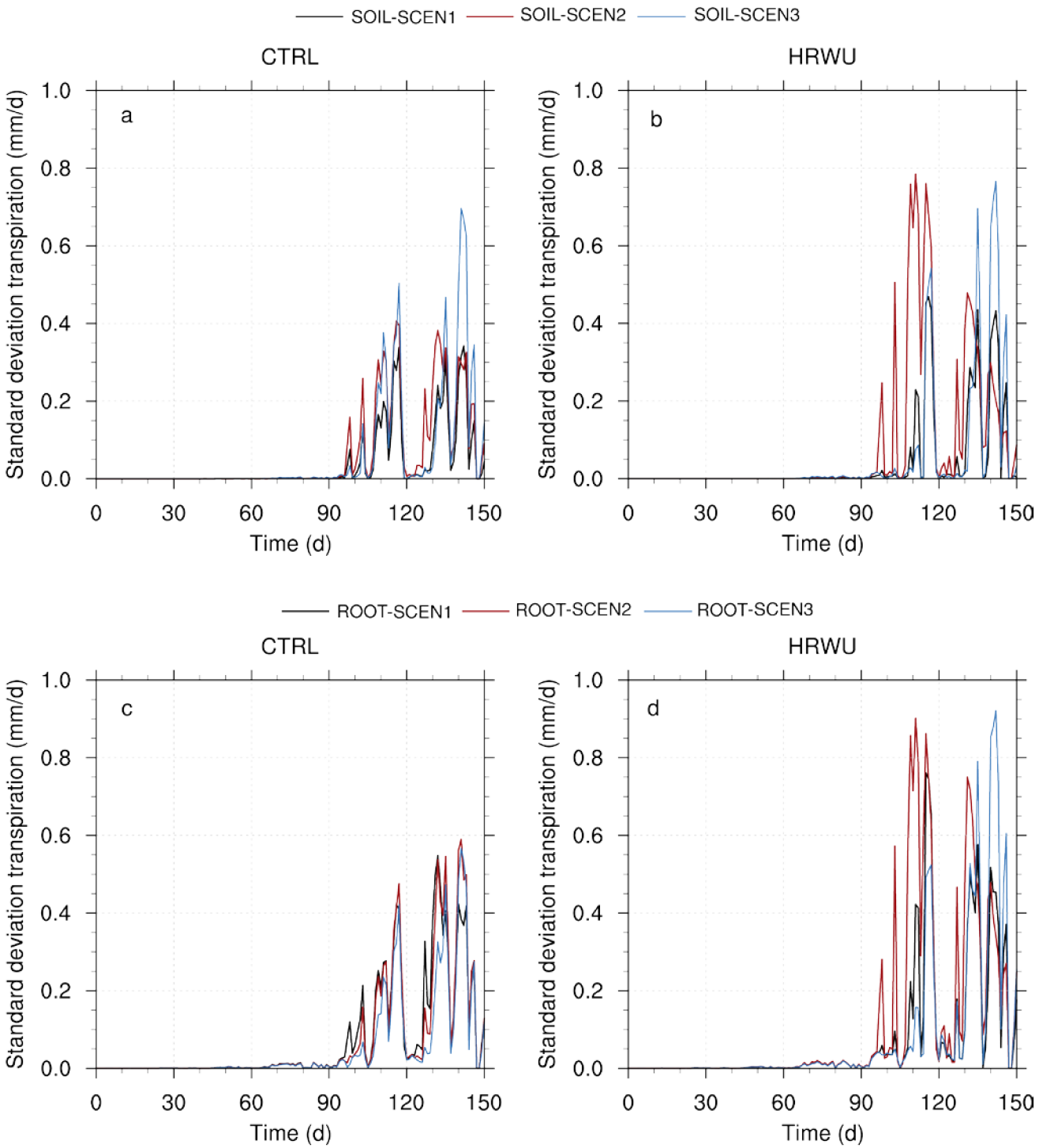

Figure 12: Time evolution of the standard deviation of the transpiration fluxes within the SOIL (top) and ROOT (bottom) group for the CTRL (left) and HRWU (right) model(s). The standard deviation of each SOIL and ROOT member represents the dispersion between the transpiration fluxes of the root and soil scenarios, respectively.

	SOIL	ROOT
FULL-PERIOD (0-150 d)	0.011	0.1039
STRESS-PERIOD (105-119 d; 130-145 d)	0.032	0.438

Table 3: Significant (below 0.01) coefficient of multiple determination (R^2 from a one-way ANOVA of the difference (i.e., CTRL-HRWU) between the transpiration fluxes for the SOIL and ROOT treatments. Values are obtained considering the complete time period and time windows where crops are susceptible to water stress conditions.

soil layers (see details in Supplement 1). The variability induced by changing the root distributions and soil parameterizations is to a large extent consistently reproduced between the two RWU formulations across the SOIL and ROOT scenarios. Subtle but significant differences, however, can be detected in the analysis of the SOIL scenarios. In particular, slightly lower standard deviation is induced by the perturbation of the root fractions at the first soil layers (i.e., 2.792 and 6.225 cm) and a remarkably larger deviation (especially for SOIL-SCEN2) at the bottom layer (i.e., 61.975 cm) in the HRWU model. These are the soil depths mainly affected by the compensatory and the HR process, which supports the findings of a previous study by Siqueira et al. [2008] and Katul and Siqueira [2010] suggesting that the effectiveness of the HR is mainly controlled by the root vertical distribution.

Finally, a one-way analysis of variance (ANOVA, see Appendix C) was performed in order to evaluate the role of root against soil parameters in explaining the difference in the transpiration flux and soil water content between the two RWU models. In particular, the ANOVA was applied to the difference of CTRL and HRWU transpiration fluxes, eliminating the temporal variability, and evaluating the three SOIL and ROOT scenarios described in section 2.3 as two groups of treatments. Moreover, the analysis was repeated considering the entire simulation period and

	LAYER 2 [2.792 cm]	LAYER 3 [6.225 cm]	LAYER 4 [11.886 cm]	LAYER 5 [21.219 cm]	LAYER 6 [36.606 cm]	LAYER 7 [61.975 cm]
SOIL	0.038 (0.109)	0.047 (0.172)	0.081 (0.288)	0.092 (0.304)	0.157 (0.452)	0.026 (0.090)
ROOT	0.134 (0.224)	0.180 (0.327)	0.224 (0.353)	0.168 (0.286)	0.060 (0.225)	0.228 (0.579)

Table 4: Significant (below 0.01) coefficient of multiple determination (R^2 from a one-way ANOVA of the difference (i.e., CTRL-HRWU) between the soil water content at different layers for the SOIL and ROOT treatments. Values are obtained considering the complete time period and time windows where crops are susceptible to water stress conditions (values in brackets).

the two limited time windows (i.e., 105-119 d and 130-145 d) when plants were susceptible to water-stress. Table 3 contains the resulting coefficient of determination (R^2) with a 0.01 significance level tested with a *F* test. Large values of R^2 indicate that a large part of the total variability is induced by the respective treatment, assuming a linear relationship. The results clearly highlight the dominant role of the ROOT parameters in explaining the difference between the CTRL and HRWU model, especially under drier soil conditions. The ANOVA was repeated for soil water content differences between CTRL and HRWU, simulated at different layers between 2.79 and 61.97 cm soil depth (Table 4). Results of R^2 confirm that the ROOT parameters largely explain the variance in the difference between CTRL and HRWU model response for most of the soil layers. The model layer at which the SOIL parameters explains most of the variability coincides with minor differences between the ROOT scenarios.

4 Parameterization of the HRWU model

In ESMs, the physiological characteristics of the vegetation are defined via a lookup table containing the parameters values describing the aerodynamic, optical, rooting depth, and

791 photosynthesis properties of the individual plant functional types. For many ESMs, these
792 parameters are assumed homogeneous in space and constant in time, assumptions which are
793 retained also for the newly introduced plant hydraulic properties of the HRWU model. In the
794 present study, the use of an experimental setup based on the detailed measurements of the
795 minirhizotron facility allowed the characterization of the plant hydraulic parameters whose
796 uncertainties are major drivers of variability in the model response [Feddes et al., 2001], as
797 shown in the sensitivity analysis of section 3.1. Therefore, the application of the HRWU model
798 over different setups, including also large domains with heterogeneous land cover and
799 undersampled but climatically important regions, poses the challenging task of identifying a set
800 of representative hydraulic parameters for each plant functional type. In this context, different
801 feasible approaches how to parameterize the HRWU model are outlined in the following
802 paragraph. While these different approaches have been identified according to previous studies
803 focused on the analysis of processes at the plant scale, their effectiveness in providing
804 representative root hydraulic properties over a generic plant category classification, as implied
805 in the definition of PFTs, would require further work. In particular, such generic PFT hydraulic
806 parameters could be cross-validated with values obtained from proxy plant characteristics
807 extracted from globally assembled databases of plant traits, e.g., Global Plant Trait Network
808 [Wright et al., 2004] and TRY [Kattge et al., 2011] and by exploiting emerging trait correlations
809 determined by physical constraints as well as those reflecting strategic plant trade-offs (e.g., the
810 coordination between the root in terms of root hydraulic conductance and the shoot as reflected
811 in the stomatal conductance), as recently outlined by Kueppers et al. [2016] for improving PFTs
812 parameterizations in ESMs.

813

814 An approach for assessing root system hydraulic parameters consists in the mathematical
815 modeling of the plant hydraulic architecture. This approach was previously implemented by

816 Couvreur et al. [2012; 2014b] for maize and winter wheat based on root architectures
817 reconstructed with the root growth model RootTyp [Pages et al., 1989]. In their study, literature
818 data on root growth rates, branching patterns, angles, etc. for each root type were
819 complemented by root length density and plant density data to create realistic architectures.
820 Root radial and axial hydraulic data for each root type were then used to calculate K_{rs}
821 mathematically. Recently, a web application (MARSHAL;
822 https://plantmodelling.shinyapps.io/marshal/) has been developed in order to automatically
823 generate realistic root system architectures with the root growth model CRootBox [Schnepf et
824 al., 2018] and to calculate directly K_{rs} and K_{comp} as separate parameters. This novel workflow,
825 which is also suitable for the coupling with sensitivity analysis algorithms, has been tested for
826 maize crop by Meunier et al. [2016] using observed hydraulic conductivities of the full crop cycle
827 reported in literature. Values obtained by implementing this web application range between 10^{-8}
828 and $4 \cdot 10^{-7}$ $m \cdot s^{-1} \cdot MPa^{-1}$ for 30 to 70 days old maize plants matching measured root length
829 densities and assuming 9 plants per square meter. This mathematical parameterization
830 approach is also a viable solution when root system architecture is measured directly from
831 rhizotrons or computed tomography scans. The second approach envisioned for the HRWU
832 parameterization by Couvreur et al. [2014a] is the direct translation of parameter tables from a
833 widely used RWU model [Feddes et al., 1978], for which libraries are available in both LSMs
834 and crop models. While the equations of these two models differ, they both base their
835 parametrization on a soil water potential at which stomata start to close (called *smpso* in LSMs
836 and h_2 in crop models), and a soil water potential at which water may not be extracted from the
837 soil (called *smpsc* in LSMs and h_3 in crop models). Following Couvreur et al. [2014a], K_{rs} in
838 isohydric plants equals $\frac{T_{pot}}{h_2 - h_3}$. Parameter tables from Wesseling et al. [1991] or Leng et al.
839 [2016] yield K_{rs} values of $6 \cdot 10^{-8}$ to 1.5 10^{-7} $m \cdot s^{-1} \cdot MPa^{-1}$ for maize, which are in the range
840 estimated with MARSHAL [Meunier, 2017]. This second approach could be crucial as it is the

most straightforward and because the possibilities of parameterization via the aforementioned mathematical modeling approach are limited or costly for some plants such as trees. Inverse modeling techniques could be identified as a third solution to estimate effective properties that are hardly measurable, such as hydraulic properties representative for the plant and soil at the field scale. In these techniques, parameter values that yield the best match between simulated and observed variables are assumed optimal. For instance, this was implemented from combined modeling and observations of deuterated lupine root water uptake in a rhizotron [Zarebanadkouki et al., 2016], the modeling and observation of water isotopologues uptake by ryegrass roots in a rhizotron [Meunier et al., 2017b], and the modeling and observation of soil water dynamics in a winter wheat field [Cai et al., 2017]. The aforementioned inverse modeling studies focused on the estimation of the hydraulic properties of root segments or the hydraulic properties of the entire root system. Also the root distribution, which reflects the range of depths from which plants can extract water, is an important characteristic of the hydraulic root architecture. Inverse modeling approaches have been used for the global estimation of plants rooting depth by Schenk and Jackson [2005], Schenk [2008], Gao et al. [2014], and Fan et al. [2017] as a function of local climate, soil properties, and groundwater levels. In addition to adapting the rooting depth to the environment, also root density affects the plants water uptake capacity. Cai et al. [2018] showed that, for the same minirhizotron facility used in our study, the relations between root system properties (root density and depth) were important to explain the effect of the adaptation of root systems to soil and meteorological conditions (e.g. drought stressed versus well-watered) on the root system water uptake capacity. Finally, the direct measurement of K_{rs} with a high-pressure flow meter [e.g., Tyree et al., 1996] or a pressure chamber [Miyamoto et al., 2001; Parent et al., 2009; Alsina et al., 2011; Caldeira et al., 2014] could be identified as the fourth viable approach to parameterize the model. While these approaches have also the advantage of providing a detailed characterization of the variability of

866 the hydraulic traits within the same population of plants, their application at regional and/or
867 global scale remains elusive as it requires the deployment of large-scale monitoring networks.

868 5 Summary and conclusions

869 This work presented the integration of a macroscopic RWU model based on the hydraulic
870 architecture approach (HRWU) in the land surface component, CLM (version 4.0), of a
871 terrestrial systems modeling platform. The model is based on three macroscopic parameters,
872 namely, the compensatory RWU conductance, the root system equivalent conductance, and the
873 leaf water potential at stomatal closure, which implicitly account for the full root system hydraulic
874 architecture and its regulation on the transpiration process. The proposed RWU scheme was
875 tested by performing point-scale numerical simulations based on the detailed information of a
876 sheltered minirhizotron facility located in Selhausen, Germany. Specifically, the model was
877 parameterized for a generic crop plant functional type according to continuous monitoring of the
878 plant growth process (i.e., rooting depth) and using crop hydraulic characteristics retrieved from
879 inverse modeling with a soil-plant hydraulic model setup for the same study site. Model results
880 were compared against sap flow transpiration fluxes and soil moisture content measured at
881 different depths using time-domain reflectometry sensors and benchmarked with the standard
882 RWU scheme (CTRL) implemented in CLM. Sensitivity numerical experiments were also
883 conducted in order to take into account the uncertainty in the parameterization of crop
884 physiological properties as well as their interplay with soil hydraulic characteristics.

885

886 The results showed plausible response for both RWU schemes when compared to the available
887 measurements of transpiration and soil moisture when using the reference soil scenario that
888 more closely reflects the standard implementation of CLM. In particular, summarizing statistics

889 of the Taylor diagram indicated a good agreement in terms of phase, slight overestimation of
890 temporal variability, and larger values for the normalized root-mean-square error of the
891 simulated transpiration. Poorer performances were obtained for the simulated soil moisture,
892 which was mainly related to a strong underestimation of the standard deviation due to the
893 adjustment from the coarsed-interpolated initial conditions. Notably, similar performance
894 statistics were found for the CTRL model configuration, except for the soil layer with a larger
895 fraction of roots where the HRWU model outperforms the CTRL configuration. However, an
896 analysis of the model performance statistics obtained using different soil scenarios indicated a
897 strong dependence of both model skills to the adopted soil parameterization. This implies that
898 differences in performance statistics between the two RWU formulations were minor if
899 compared to those reflecting different soil characteristics scenarios. The qualitative analysis of
900 the simulated transpiration fluxes and the water limiting factors identified water stress conditions
901 as periods when substantial differences were detected between the CTRL and the HRWU
902 approach, the latter matching better with the sap flow measurements. Moreover, a visual
903 inspection of the time evolution of the vertical profile of soil moisture showed the role of the
904 hydraulic compensation in taking up more water from the deeper soil layers and the
905 redistribution of water from deeper to shallower soil layers by HR process, which explained the
906 slightly higher transpiration simulated by the HRWU model after prolonged dry conditions due to
907 the sheltering of the facility. Quantitative differences between the two RWU models were around
908 2-7% of the total transpiration measured by the sap flow sensors, with about 13-17% variations
909 among the different HRWU model scenarios reflecting the impact of the large uncertainty
910 associated to its hydraulic parameterization.

911

912 The sensitivity of the HRWU model to the newly introduced physiological parameters was
913 assessed by using values retrieved from literature for the leaf water potential at stomatal closure

914 and values reflecting different growth stages of the plant for the root system equivalent
915 conductance. Results showed the important role played by the new parameters in modulating
916 the transpiration and soil moisture distribution after prolonged dry conditions. The results of this
917 sensitivity analysis provided also a mechanistic interpretation of the HRWU model response.
918 Specifically, the range of soil matric potentials generating water limitation is extended up to
919 wetter soil conditions if the root equivalent conductance is sufficiently low while the range of soil
920 matric potential generating water limitation is translated when changing the leaf water potential.
921 Finally, an analysis of variability across the soil and root scenarios indicated that differences in
922 soil water content are mostly simulated through the root distribution, while the transpiration flux
923 in both RWU models is additionally determined through the soil characteristics.

924

925 Overall, the effort presented in this work is well aligned with the improvements contained in the
926 recent release of CLM (version 5.0) representing a plant hydraulic stress and emphasized in the
927 roadmap discussed in Rogers et al. [2017] for improving the photosynthesis process in ESMs.
928 The insights gained using the experimental setup of this study highlight, however, the need of
929 performing large scale (i.e., continental/global) simulations spanning longer time periods,
930 contrasting climate regimes, and vegetation types characterized by different physiological
931 properties. These efforts will serve as basis (i) for verifying to which extent inversely calculated
932 plant hydraulic parameters apply to a generic PFT classification as well as (ii) for a sound
933 evaluation of the HRWU model response according to the parameterization approaches outlined
934 in section 4. These large-scale simulations will give also the opportunity to better substantiate
935 the response of the proposed HRWU scheme with emerging plant properties (e.g., evaporation-
936 transpiration partitioning) retrieved from extended monitoring networks and remote sensing
937 products of ecosystem fluxes. In this context, the implementation within a coherent modeling
938 framework of different RWU approaches and plant water stress formulations appears relevant

for providing a strong basis for the development of ad-hoc intercomparison studies. These initiatives are the foundation for a systematic quantification of the uncertainty associated to the estimation of the transpiration fluxes in ESMs during drought periods.

Acknowledgments

This research work was supported by the SFB/TR32 Patterns in Soil-Vegetation-Atmosphere Systems: Monitoring, Modeling and Data Assimilation project funded by the Deutsche Forschungsgemeinschaft (DFG) and by the Terroir Future–Impact of Climate Change on Viticulture in Luxembourg: Risk-Assessment and Potential Adaptation Strategies project financed by the Institute Viti-Vinicole. Valentin Couvreur was supported by the Interuniversity Attraction Poles Programme-Belgian Science Policy (grant IAP7/29). We would like to thank Alexander Graf for providing meteorological data from the Eifel/Lower Rhine valley observatory of the TERENO project funded by the Helmholtz Association, Matthias Langensiepen for post-processing and providing the sap flow data, and Sidney Marschollek for the valuable feedbacks on the integration of the hydraulic model in CLM. We also gratefully acknowledge the computing time (project HBN33) granted by the John von Neumann Institute for Computing (NIC) and provided on the supercomputer JURECA at the Juelich Supercomputing Centre (JSC). The constructive criticism of two anonymous reviewers has been greatly beneficial for the quality of the manuscript.

Appendix

A. Pedotransfer functions

The soil hydraulic properties are determined from soil texture (i.e., sand and clay contents) based on the work of Clapp and Hornberger [1978] and Cosby et al. [1984]. According to these formulations the porosity of the mineral soil is calculated as

$$\theta = 0.489 - 0.00126 \cdot (\%sand), \quad \text{(A.1)}$$

the saturated hydraulic conductivity is equal to

$$K_{sat} = 0.0070556 \cdot 10^{-0.884+0.0153 \cdot (\%sand)}, \quad \text{(A.2)}$$

the saturated soil matric potential is

$$\psi_{sat} = -10.0 \cdot 10^{1.88-0.0131 \cdot (\%sand)}, \quad \text{(A.3)}$$

and the exponent of the soil characteristic curve is estimated as

$$b = 2.91 + 0.159 \cdot (\%sand). \quad \text{(A.4)}$$

Note that in the complete formulation the pedotransfer functions are modified to consider the soil organic content. This is, however, not taken into account in the parameterization of the model for the minirhizotron facility.

B. Inverse and forward calculation of K_{rs}

To compare the values of K_{rs} derived from the architecture model (i.e., forward approach) and from the inverse modeling, the units of the two conductances (architecture model: conductance of a single plant given in $cm^3\ hPa^{-1}\ d^{-1}$, inverse modeling: conductance of the root system below a unit surface area given in h^{-1}) had to be matched. Therefore, pressure differences were

expressed in terms of pressure heads (cm) and the conductance was normalized by the total root length so as to obtain the conductance per unit of root length: cm h^{-1}, which was from cm^3 h^{-1} (transpiration rate) cm^{-1} (pressure head difference) cm^{-1} (root length). The conductance derived from the architecture model, K_{rs_Fd}, had to be divided by the total root length of a plant RL_{Fd} / *plant*: $K_{rs} = K_{rs\_Fd} / (RL_{Fd} / plant)$. The conductance obtained from the inverse modeling K_{rs_IV} had to be divided by the total root length under one unit of soil surface area (*A*) RL_{IV} / A. The latter total root length corresponds with the depth integral of the root length density (RLD). Therefore, observations of roots in the rhizotubes were transformed to RLDs. However, there are two ways to calculate the total root length according to Cai et al. [2016]. One assuming that the root length obtained from the volume of multiplying the area of the root image by the view depth of the camera. The other one assuming that the roots would grow nearly vertically in absence of the rhizotube, in a soil volume with height, width, and depth respectively equal to the diameter, radius of the rhizotube, and width of the image, the projected root length equals the number of intercepted roots times by the diameter of the rhizotube. Therefore, for the conductance obtained from the inverse modeling, $K_{rs}' = K_{rs\_IV} / (RL_{IV\_1} / A)$ or $K_{rs}'' = K_{rs\_IV} / (RL_{IV\_2} / A)$. The values of K_{rs} from the forward calculation is $1.48 \cdot 10^{-7}$ cm h^{-1} while K_{rs}' and K_{rs}'' obtained from the inverse modeling using the two methods to obtaining the total root length are $1.54 \cdot 10^{-8}$ cm h^{-1} and $1.26 \cdot 10^{-7}$ cm h^{-1}, respectively, after converting the unit.

C. Analysis of variance

A one-way analysis of variance (ANOVA; von Storch and Zwiers, [1999]) is used to examine the role of SOIL and ROOT parameters on the variability of the transpiration flux and soil water content differences between HRWU and CTRL. The ANOVA is a generalization of the student's *t* test with more than two treatments (ROOT and SOIL), based on *J* samples (3 scenarios each) of size *n* (number of days being evaluated), represented by random variables Y_{ij} for i = 1,…,*n*

and j = 1,...,J. Here, Y_{ij} represents the difference of the transpiration flux and soil water content as HRWU-CTRL, respectively. With element i of sample j, we can define a linear statistical model

$$Y_{ij} = \mu + a_j + \varepsilon_{ij} \quad \text{(B.1)}$$

to examine the variability of the transpiration flux and soil water content differences (Y_{ij}) due to the SOIL and ROOT parameters. The mean of each sample is described by $\mu = \frac{1}{J}\sum_{j=1}^{J}\mu_j$ and the coefficients $a_j = \mu_j - \mu$ describe the treatment effect (i.e., the linear relationship between the mean and the ROOT and SOIL scenarios, respectively). The statistical error is described by $\varepsilon_{ij} \sim N(0, \sigma^2)$.

The total variability of this statistical model is then defined by the total sum of squares

$$SST = \sum_{i=1}^{n}\sum_{j=1}^{J}(Y_{ij} - Y_{oo})^2 \quad \text{(B.2)}$$

and can be decomposed into a treatment sum of squares

$$SSA = n\sum_{j=1}^{J}(Y_{oj} - Y_{oo})^2, \quad \text{(B.3)}$$

which defines the variability induced by ROOT and SOIL parameters. Here, Y_{oo} is the unbiased estimator of μ and the notation "o" indicates the average over the missing subscript. Additionally, we consider the sum of squared errors

$$SSE = n\sum_{j=1}^{J}(Y_{ij} - Y_{oj})^2 \quad \text{(B.4)}$$

to calculate the adjusted coefficient of multiple determination for the SOIL and ROOT parameters, i.e.

$$R^2 = \frac{SSA - \frac{J-1}{J(n-1)} SSE}{SST}. \quad \text{(B.5)}$$

R^2 ranges from 0 to 1 and indicates the proportion of variability in the response variable (differences of the transpiration flux and soil water content as HRWU-CTRL) induced by the treatment (SOIL and ROOT parameters), assuming a linear relationship. The higher R^2, the more variability is induced by the SOIL or ROOT parameters, respectively.

D. Supplementary data

The following is Supplementary data to this article:

References

Aanderud Z.T., and J. H. Richards, Hydraulic redistribution may stimulate decomposition, *Biogeochemistry,* 95: 323–333, doi: 10.1007/s10533-009-9339-3, 2009.

Alsina M. M., Smart D.R., Bauerle T., et al. Seasonal changes of whole root system conductance by a drought-tolerant grape root system. *J. Exp. Bot*., 62(1): 99-109, doi: 10.1093/jxb/erq247, 2011.

Amenu, G. G. and P. Kumar. A model for hydraulic redistribution incorporating coupled soil-root moisture transport, *Hydrol. Earth Syst. Sci*., 12, 55-74, doi:10.5194/hess-12-55-2008, 2008.

Baram, S., V. Couvreur, T. Harter, M. Read, P.H. Brown, M. Kandelous, D.R. Smart, and J.W. Hopmans, Estimating Nitrate Leaching to Groundwater from Orchards: Comparing Crop Nitrogen Excess, Deep Vadose Zone Data-Driven Estimates, and HYDRUS Modeling. *Vadose Zone J*., 15. doi:10.2136/vzj2016.07.0061, 2016.

Bohrer, G., H. Mourad, T. A. Laursen, D. Drewry, R. Avissar, D. Poggi, R. Oren, and G. G. Katul, Finite element tree crown hydrodynamics model (FETCH) using porous media flow within branching elements: A new representation of tree hydrodynamics, *Water Resour. Res*., 41, W11404, doi:10.1029/2005WR004181, 2005.

Bonan, G. B., Land–atmosphere CO_2 exchange simulated by a land surface process model coupled to an atmospheric general circulation model, *J. Geophys. Res*., 100(D2), 2817-2831, doi:10.1029/94JD02961, 1995.

Bonan, G. B., M. Williams, R. A. Fisher, and K. W. Oleson, Modeling stomatal conductance in the earth system: linking leaf water-use efficiency and water transport along the soil–plant–atmosphere continuum, *Geosci. Model Dev*., 7, 2193-2222, doi:10.5194/gmd-7-2193-2014, 2014.

1066 Bouda M., and J. E. Saiers, Dynamic effects of root system architecture improve root water
1067 uptake in 1-D process-based soil-root hydrodynamics, *Adv. Water Resour.*, 110, 319-334 doi:
1068 10.1016/j.advwatres.2017.10.018, 2017.

1069 Burgess, S. S. O., M. A. Adams, N. C. Turner, C. K. Ong, The redistribution of soil water by tree
1070 root systems, *Oecologia* 115: 306–311, doi: 10.1007/s004420050521, 1998.
1071
1072 Cai, G., J. Vanderborght, A. Klotzsche, J. van der Kruk, J. Neumann, N. Hermes, and H.
1073 Vereecken, Construction of minirhizotron facilities for investigating root zone processes, *Vadose*
1074 *Zone J.,* 15(9), doi:10.2136/vzj2016.05.0043, 2016.

1075 Cai, G., J. Vanderborght, V. Couvreur, C.M. Mboh, and H. Vereecken, Parameterization of root
1076 water uptake models considering dynamic root distributions and water uptake compensation.
1077 *Vadose Zone J.* doi:10.2136/vzj2016.12.0125, 2017.

1078 Cai, G., J. Vanderborght, M. Langensiepen, A. Schnepf, H. Huging and H. Vereecken. Root
1079 growth, water uptake, and sap flow of winter wheat in response to different soil water conditions.
1080 *Hydrol. Earth Syst. Sci.*, 22,(4), 2449-2470, doi: 10.5194/hess-22-2449-2018, 2018.

1081 Caldeira, C. F., M. Bosio, B. Parent, L. Jeanguenin, F. Chaumont, and F. Tardieu, A Hydraulic
1082 Model Is Compatible with Rapid Changes in Leaf Elongation under Fluctuating Evaporative
1083 Demand and Soil Water Status, *Plant Physiology*, 164 (4) 1718-1730; doi:
1084 10.1104/pp.113.228379, 2014.

1085 Caldeira, C. F., L. Jeanguenin, F. Chaumont, and F. Tardieu, Circadian rhythms of hydraulic
1086 conductance and growth are enhanced by drought and improve plant performance, *Nat.*
1087 *Commun.* 5:5365, doi: 10.1038/ncomms6365, 2014.

1088

1089 Caldwell M. M., T. E. Dawson J. H. Richards, Hydraulic lift: consequences of water efflux from
1090 the roots of plants, *Oecologia* 113: 151–161, doi: 10.1007/s004420050363, 1998.

1091 Clapp, R. B., and G. M. Hornberger, Empirical equations for some soil hydraulic properties,
1092 *Water Resour. Res*., 14(4), 601–604, doi:10.1029/WR014i004p00601, 1978.

1093 Combe, M., de Arellano, J. V. G., Ouwersloot, H. G., and Peters, W., Plant water-stress
1094 parameterization determines the strength of land-atmosphere coupling. *Agric. For. Meteorol*.,
1095 217,61–73, doi: 10.1016/j.agrformet.2015.11.006, 2016.

1096 Cosby, B. J., G. M. Hornberger, R. B. Clapp, and T. R. Ginn, A Statistical Exploration of the
1097 Relationships of Soil Moisture Characteristics to the Physical Properties of Soils, *Water Resour.*
1098 *Res.*, 20(6), 682–690, doi:10.1029/WR020i006p00682, 1984.

1099 Couvreur, V., J. Vanderborght, and M. Javaux. A simple three-dimensional macroscopic root
1100 water uptake model based on the hydraulic architecture approach, *Hydrol. Earth Syst. Sci*., 16,
1101 2957-2971, doi:10.5194/hess-16-2957-2012, 2012.

1102 Couvreur, V., J. Vanderborght, X. Draye, and M. Javaux, Dynamic aspects of soil water
1103 availability for isohydric plants: Focus on root hydraulic resistances, *Water Resour. Res*., 50,
1104 8891–8906, doi:10.1002/2014WR015608, 2014.

1105 Couvreur, V., J. Vanderborght, L. Beff, and M. Javaux, Horizontal soil water potential
1106 heterogeneity: simplifying approaches for crop water dynamics models, *Hydrol. Earth Syst. Sci*.,
1107 18, 1723-1743, doi: 10.5194/hess-18-1723-2014, 2014.

1108 Daly, E., A. Porporato, and I. Rodriguez-Iturbe, Coupled dynamics of photosynthesis,
1109 transpiration, and soil water balance. Part I: Upscaling from hourly to daily level, *J.*
1110 *Hydrometeorol*., 5(3), 546-558, doi: 10.1175/1525-7541(2004)005<0546:CDOPTA>2.0.CO;2,
1111 2004.

1112 Damour, G., T. Simonneau, H. Cochard, and L. Urban, An overview of models of stomatal
1113 conductance at the leaf level, *Plant, Cell & Environment*, 33: 1419-1438. doi:10.1111/j.1365-
1114 3040.2010.02181.x, 2010.

1115 De Kauwe, M. G., J. Kala, Y.-S. Lin, A. J. Pitman, B E. Medlyn, R. A. Duursma, G. Abramowitz,
1116 Y.-P. Wang, and D. G. Miralles, A test of an optimal stomatal conductance scheme within the
1117 CABLE land surface model, *Geosci. Model Dev.*, 8, 431-452, doi:10.5194/gmd-8-431-2015,
1118 2015a.

1119 De Kauwe, M. G., S.-X. Zhou, B. E. Medlyn, A. J. Pitman, Y. P. Wang, R. A. Duursma, and I. C.
1120 Prentice, Do land surface models need to include differential plant species responses to
1121 drought? Examining model predictions across a latitudinal gradient in Europe, *Biogeosciences*,
1122 12, 12349–12393, doi:10.5194/bgd-12- 12349-2015, 2015b.

1123 Deckmym, G., H. Verbeeck, M. O. de Beeck, D. Vansteenkiste, K. Steppe, and R. Ceulemans,
1124 ANAFORE: A stand-scale process-based forest model that includes wood tissue development
1125 and labile carbon storage in trees, *Ecol. Model.*, 215, 345-368,
1126 doi:10.1016/j.ecolmodel.2008.04.007, 2008.

1127 Diffenbaugh N. S. and C. B. Field, Changes in ecologically critical terrestrial climate conditions,
1128 *Science*, 341, 486-492, doi: 10.1126/science.1237123, 2013.

1129 Domec, J.-C., J. S. King, A. Noormets, E. Treasure, M. J. Gavazzi, G. Sun, and S. G.
1130 McNulty, Hydraulic redistribution of soil water by roots affects whole-stand
1131 evapotranspiration and net ecosystem carbon exchange, *New Phytol.*, 187: 171–183.
1132 doi:10.1111/j.1469-8137.2010.03245.x, 2010.

1133

1134 Doussan, C., A. Pierret, E. Garrigues, and L. Pages, Water uptake by plant roots: II - Modelling
1135 of water transfer in the soil root-system with explicit account of flow within the root system -
1136 Comparison with experiments, *Plant Soil*, 283: 99, doi: 10.1007/s11104-004-7904-z, 2006.

1137 Drewry, D. T., P. Kumar, S. Long, C. Bernacchi, X.-Z. Liang, and M. Sivapalan , Ecohydrological
1138 responses of dense canopies to environmental variability: 1. Interplay between vertical structure
1139 and photosynthetic pathway. *J Geophys Res.*, 115, doi: 10.1029/2010JG001340, 2010.

1140 Egea, G., A. Verhoef, and P. L. Vidale, Towards an improved and more flexible representation
1141 of water stress in coupled photosynthesis–stomatal conductance models, *Agric. For. Meteorol.*,
1142 151, 1370-1384, doi: 10.1016/j.agrformet.2011.05.019, 2011.

1143 Feddes R. A., and P.E. Rijtema, Water withdrawal by plant roots, *J. Hydrol.*,17(1–2), 33-59, doi:
1144 10.1016/0022-1694(72)90065-0, 1972.

1145 Feddes R. A., H. Hoff, M. Bruen, T. Dawson, P. de Rosnay, P. Dirmeyer, R. B. Jackson, P.
1146 Kabat, A. Kleidon, A. Lilly, and A. J. Pitman, Modeling Root Water Uptake in Hydrological and
1147 Climate Models, *Bull. Am. Meteorol. Soc.*, 82 (12), 2797-2809, doi: *10.1175/1520-*
1148 *0477(2001)082<2797:MRWUIH>2.3.CO;2,* 2001.

1149 Fan, Y., G. Miguez-Macho, E. G. Jobbágy, R. B. *Jackson*, and C. Otero-Casal, Hydrologic
1150 regulation of plant *rooting* depth, *Proc. Natl. Acad. Sci. USA*, 114(40), 10572-10577,
1151 doi:10.1073/pnas.1712381114, 2017.

1152 Fatichi, S., C. Pappas, and V. Y. Ivanov, Modeling plant-water interactions: An ecohydrological
1153 overview from the cell to the global scale, *WIREs Water*, 3(3), 327-368, doi:
1154 doi.org/10.1002/wat2.1125, 2016.

1155

1156 Foley, J.A., N. Ramankutty, K.A. Brauman, E.S. Cassidy, J.S. Gerber, M. Johnston, N.D.
1157 Mueller, C. O'Connell, D.K. Ray, P.C. West, C. Balzer, E.M. Bennett, Carpenter S.R., J. Hill, C.
1158 Monfreda, S. Polasky, J. Rockström, J. Sheehan, S. Siebert, D. Tilman, and D.P.M. Zaks,
1159 Solutions for a cultivated planet, *Nature,* 478, 337-342, doi:10.1038/nature10452, 2011.

1160 Friedlingstein, P., P. Cox, R. Betts, L. Bopp, W. von Bloh, V. Brovkin, P. Cadule, S. Doney, M.
1161 Eby, I. Fung, G. Bala, J. John, C. Jones, F. Joos, T. Kato, M. Kawamiya, W. Knorr, K. Lindsay,
1162 H.D. Matthews, T. Raddatz, P. Rayner, C. Reick, E. Roeckner, K. Schnitzler, R. Schnur, K.
1163 Strassmann, A.J. Weaver, C. Yoshikawa, and N. Zeng, Climate–Carbon Cycle Feedback
1164 Analysis: Results from the C^{4}MIP Model Intercomparison, *J. Climate*, 19, 3337–3353, doi:
1165 10.1175/JCLI3800.1, 2006.

1166 Fu, C., G. Wang, M. L. Goulden, R. L. Scott, K. Bible, and Z. G. Cardon. Combined
1167 measurement and modeling of the hydrological impact of hydraulic redistribution using CLM4.5
1168 at eight AmeriFlux sites, *Hydrol. Earth Syst. Sci*., 20, 2001-2018, doi: 10.5194/hess-20-2001-
1169 2016, 2016.

1170 Fu, C., X. Lee, T. J. Griffis, G. Wang, and Z. Wei, Influences of root hydraulic redistribution on
1171 N2O emissions at AmeriFlux sites, *Geophys. Res. Lett*., 45, 5135–5143, doi:
1172 10.1029/2018GL077789, 2018.

1173 Gao H., M. Hrachowitz, S. J. Schymanski, F. Fenicia, N. Sriwongsitanon and H. H. G. Savenije,
1174 Climate controls how ecosystems size the root zone storage capacity at catchment scale,
1175 *Geophys. Res. Lett*., 41, (22), 7916-7923, doi: 10.1002/2014GL061668, 2014.

1176 Huber, K., J. Vanderborght, M. Javaux, N. Schroder, I. C. Dodd, and H. Vereecken, Modelling
1177 the impact of heterogeneous rootzone water distribution on the regulation of transpiration by
1178 hormone transport and/or hydraulic pressure, *Plant Soil*, 384: 93, doi: 10.1007/s11104-014-
1179 2188-4, 2014.

1180 Hultine, K.R., D. G. Williams, S. S. O. Burgess, T. O. Keefer, Contrasting patterns of hydraulic
1181 redistribution in three desert phreatophytes, *Oecologia* 135: 167‑175, doi: 10.1007/s00442-002-
1182 1165-4, 2003.

1183 Jerszurki, D., V. Couvreur, T. Maxwell, L. de Carvalho Ramos Silva, N. Matsumoto, K. Shackel,
1184 J. L. Moretti de Souza, and J. Hopmans, Impact of root growth and hydraulic conductance on
1185 canopy carbon-water relations of young walnut trees (*Juglans regia L.*) under drought, *Scientia*
1186 *Horticulturae*, 226, 342-352, doi: 10.1016/j.scienta.2017.08.051, 2017.

1187 Kala, J., M. G. De Kauwe, A. J. Pitman, B. E. Medlyn, Y.-P. Wang, R. Lorenz, and S. E.
1188 Perkins-Kirkpatrick, Impact of the representation of stomata conductance on model projections
1189 of heatwave intensity, *Sci. Rep.,* 6, 23418, doi: 10.1038/srep23418, 2016.

1190 Kattge, J., S. Diaz, S. Lavorel, et al., TRY – a global database of plant traits, *Glob. Chang. Biol.*,
1191 17(9): 2905-2935, doi: 10.1111/j.1365-2486.2011.02451.x, 2011.

1192 Katul, G. G. and M. B. Siqueira, Biotic and abiotic factors act in coordination to amplify hydraulic
1193 redistribution and lift, *New Phytol.*, 187: 3–6, doi:10.1111/j.1469-8137.2010.03306.x, 2010.

1194 Klein, T., The variability of stomatal sensitivity to leaf water potential across tree species
1195 indicates a continuum between isohydric and anisohydric behaviours. *Funct. Ecol.,* 28: 1313-
1196 1320, doi: 10.1111/1365-2435.12289*,* 2014.

1197 Konings, A. G., S. C. Dekker, M. Rietkerk, and G. G. Katul, Drought sensitivity of patterned
1198 vegetation determined by rainfall-land surface feedbacks, *J. Geophys. Res.*, 116, G04008,
1199 doi:10.1029/2011JG001748, 2011.

1200

1201 Konings, A. G., A. P. Williams, and P. Gentine, Sensitivity of grassland productivity to aridity
1202 controlled by stomatal and xylem regulation, *Nat. Geosci.* 10, 284–288 doi:10.1038/ngeo2903,
1203 2018.

1204 Kueppers, L. M., C. M. Iversen, and C. D. Koven, Expanding use of plant trait observation in
1205 Earth system models, *Eos*, 97, doi:10.1029/2016EO049947, 2016

1206 Langensiepen, M., M. Kupisch, A. Graf, M. Schmidt, and F. Ewert. Improving the stem heat
1207 balance method for determining sap-flow in wheat, *Agric. For. Meteorol.*, 186, 34-42, doi:
1208 10.1016/j.agrformet.2013.11.007, 2014.

1209 Lee, J.-E., R. S. Oliveira, T. E. Dawson, and I. Fung, Root functioning modifies seasonal
1210 climate, *Proc. Natl Acad. Sci.*, 102(49), 17576-17581, doi:10.1073/pnas.0508785102, 2005.

1211 Leng, G., X. Zhang, M. Huang, Q. Yang, R. Rafique, G. R. Asrar, and L. Ruby Leung,
1212 Simulating county-level crop yields in the Conterminous United States using the Community
1213 Land Model: The effects of optimizing irrigation and fertilization, *J. Adv. Model. Earth Syst.*, 8,
1214 1912–1931, doi: 10.1002/2016MS000645, 2016.

1215 Lobell, D. B., J. Roberts, W. Schlenker, N. Braun, B. B. Little, R. M. Rejesus, G. L. Hammer
1216 Greater sensitivity to drought accompanies maize yield increase in the U.S. Midwest, *Science*,
1217 344, 516–519, doi: 10.1126/science.1251423, 2014.

1218 Li, L., Y.-P. Wang, Q. Yu, B. Pak, D. Eamus, J. Yan, E. van Gorsel, and I. T. Baker, Improving
1219 the responses of the Australian community land surface model (CABLE) to seasonal drought, *J.*
1220 *Geophys. Res.*, 117, G04002, doi:10.1029/2012JG002038, 2012.

1221

1222 Liu, Y., S. Piao, X. Lian, P. Ciais, and W.K. Smith, Seasonal Responses of Terrestrial Carbon
1223 Cycle to Climate Variations in CMIP5 Models: Evaluation and Projection, *J. Climate*, 30, 6481–
1224 6503, doi: 10.1175/JCLI-D-16-0555.1, 2017.

1225 Manzoni, S., G. Vico, G. Katul, S. Palmroth, and A. Porporato, Optimal plant water-use
1226 strategies under stochastic rainfall, *Water Resour. Res.*, 50, doi:10.1002/2014WR015375, 2014

1227 Martin-StPaul, N., S. Delzon, and H. Cochard, Plant resistance to drought depends on timely
1228 stomatal closure. *Ecol. Lett*. 20, 1437-1447, doi: 10.1111/ele.12851, 2017.

1229 McDermid, S. S., L. O. Mearns, and A. C. Ruane, Representing agriculture in Earth System
1230 Models: Approaches and priorities for development, *J. Adv. Model. Earth Syst.*, 9, 2230–2265,
1231 doi:10.1002/2016MS000749, 2017.

1232 McDowell, N., W. T. Pockman, C. D. Allen, D. D. Breshears, N.Cobb, T. Kolb, J. Plaut, J.
1233 Sperry, A. West, D. G. Williams, and E. A. Yepez, Mechanisms of plant survival and mortality
1234 during drought: why do some plants survive while others succumb to drought?, *New Phytol.*,
1235 178: 719–739. doi:10.1111/j.1469-8137.2008.02436.x, 2008.

1236 Medlyn, B. E., R. A. Duursma, D. Eamus, D. S. Ellsworth, I. C. Prentice, C. V. M. Barton, K. Y.
1237 Crous, P. De Angelis, M. Freeman, and L. Wingate, Reconciling the optimal and empirical
1238 approaches to modelling stomatal conductance, *Global Change Biol.*, 17, 2134–2144,
1239 0.1111/j.1365-2486.2010.02375.x, 2011.

1240 Meunier F., V. Couvreur, M. Javaux, and J. Vanderborght, A new model for optimizing the water
1241 acquisition of root hydraulic architectures over full crop cycles, IEEE, 140-149,
1242 doi:10.1109/FSPMA.2016.7818300, 2016.

1243

1244 Meunier, F. Revisiting crop root systems ideotypes for water uptake - New tools and models.
1245 PhD Thesis, Université catholique de Louvain (UCLouvain), Louvain-la-Neuve, Belgium, 2017.

1246 Meunier, F., V. Couvreur, X. Draye, J. Vanderborght and M. Javaux, Towards quantitative root
1247 hydraulic phenotyping: novel mathematical functions to calculate plant-scale hydraulic
1248 parameters from root system functional and structural traits. *J. Math. Biology*, 75 (5), 1133-
1249 1170, doi: 10.1007/s00285-017-1111-z, 2017a.

1250 Meunier, F., Y. Rothfuss, T. Bariac, P. Biron, P. Richard, J.-L. Durand, V. Couvreur, J.
1251 Vanderborght, and M. Javaux, Measuring and modeling hydraulic lift of *Lolium multiflorum* using
1252 stable water isotopes, *Vadose Zone J*. doi:10.2136/vzj2016.12.0134, 2017b.

1253 Meunier F., X. Draye, J. Vanderborght, M. Javaux, and V. Couvreur, A hybrid analytical-
1254 numerical method for solving water flow equations in root hydraulic architectures, *Applied*
1255 *Mathematical Modelling*, 52, 648-663, doi: 10.1016/j.apm.2017.08.011, 2017c.

1256 Meunier, F., V. Couvreur, X. Draye, M. Zarebanadkouki, J. Vanderborght and M. Javaux, Water
1257 movement through plant roots - exact solutions of the water flow equation in roots with linear or
1258 exponential piecewise hydraulic properties, *Hydrol. Earth Syst. Sci.*, 21(12), 6519-6540, doi:
1259 10.5194/hess-21-6519-2017, 2017d.

1260 Meunier, F., M. Zarebanadkouki, M.A. Ahmed, A. Carminati, V. Couvreur and M. Javaux,
1261 Hydraulic conductivity of soil-growth lupine and maize unbranched roots and maize root-shoot
1262 junctions, *J. Plant Physiol.*, 227, 31-44, doi: 10.1016/j.jplph.2017.12.019, 2018.

1263 Miyamoto, N., E. Steudle, T. Hirasawa, and R. Lafitte, Hydraulic conductivity of rice roots, *J.*
1264 *Exp. Bot.*, 52:1835–1846, doi:10.1093/jex-bot/52.362.1835, 2001.

1265 Neumann, R. B. and Z. G. Cardon, The magnitude of hydraulic redistribution by plant roots: a
1266 review and synthesis of empirical and modeling studies, *New Phytol.*, 194: 337–352.
1267 doi:10.1111/j.1469-8137.2012.04088.x, 2012.

1268 Oleson, K. W., D. M. Lawrence, G. B. Bonan, M. G. Flanner, and E. Kluzek, Technical
1269 description of version 4.0 of the Community Land Model (CLM), *Tech. Note NCAR/TN-*
1270 *478+STR*, 257 pp., Natl. Cent. for Atmos. Res., Boulder, Colo., 2010.

1271 Oliveira R. S., T. E. Dawson, S. S. O. Burgess, and D. C. Nepstad, Hydraulic redistribution in
1272 three Amazonian trees, *Oecologia,* 145: 354–363, doi: 10.1007/s00442-005-0108-2, 2005.

1273 Pagès L., M. O. Jordan, and D. Picard, A simulation-model of the 3-dimensional architecture of
1274 the maize root-system, *Plant Soil*, 119, 147-154, doi: 10.1007/BF02370279, 1989.

1275 Parent B., C. Hachez, E. Redondo, T. Simonneau, F. Chaumont, and F. Tardieu, Drought and
1276 abscisic acid effects on aquaporin content translate into changes in hydraulic conductivity and
1277 leaf growth rate: A trans-scale approach, *Plant Physiology*, 149 (4) 2000-
1278 2012; doi: 10.1104/pp.108.130682, 2009.

1279 Parmesan, C., and G. Yohe, A globally coherent fingerprint of climate change impacts across
1280 natural systems, *Nature*, 421(6918), 37-42, doi:10.1038/nature01286, 2006.

1281 Porporato A. , F. Laio, L. Ridolfi, and I. Rodriguez-Iturbe, Plants in water-controlled ecosystems:
1282 active role in *hydrologic* processes and response to water stress III. Vegetation water stress.
1283 *Adv Water Resour*, 24:725-744, doi: 10.1016/S0309-1708(01)00006-9, 2001.

1284 Prieto I., Z. Kikvidze, F. I. Pugnaire, Hydraulic lift: soil processes and transpiration in the
1285 Mediterranean leguminous shrub *Retama sphaerocarpa* (L.) Boiss, *Plant Soil*, 329: 447‑456,
1286 doi: 10.1007/s11104-009-0170-3, 2010.

1287 Quijano, J.C., P. Kumar, D. T. Drewry, A. H. Goldstein, L. Misson, Competitive and mutualistic
1288 dependencies in multi-species vegetation dynamics enabled by hydraulic redistribution, *Water*
1289 *Resour. Res.,* 48, doi: 10.1029/2011WR011416, 2012.

1290 Quijano, J. C., P. Kumar, and D. T. Drewry, Passive regulation of soil biogeochemical cycling by
1291 root water transport, *Water Resour. Res*., 49, 3729–3746, doi: 10.1002/wrcr.20310, 2013.

1292 Quijano, J. C., and P. Kumar, Numerical simulations of hydraulic redistribution across climates:
1293 The role of the root hydraulic conductivities, *Water Resour. Res*., 51, 8529–8550,
1294 doi:10.1002/2014WR016509, 2015.

1295 Richards, J. H., and M. M. Caldwell, Hydraulic lift: Substantial nocturnal water transport between
1296 soil layers by Artemisia tridentata roots, *Oecologia* 73: 486–489, doi: 10.1007/BF00379405,
1297 1987.

1298 Ripullone F., M. R. Guerrieri, F. Magnani, and M. Borghetti Stomatal conductance and leaf
1299 water potential responses to hydraulic conductance variation in Pinus pinaster seedlings, *Trees*,
1300 21(3), 371-378, doi 10.1007/s00468-007-0130-6 2007

1301 Rogers, A., B. E. Medlyn, J. S. Dukes, G. Bonan, S. von Caemmerer, M. C. Dietze, J. Kattge, A.
1302 D. B. Leakey, L. M. Mercado, Ü Niinemets, I. C. Prentice, S. P. Serbin, S. Sitch, D. A. Way, and
1303 S. Zaehle, A roadmap for improving the representation of photosynthesis in Earth system
1304 models, *New Phytol*., 213: 22–42. doi:10.1111/nph.14283, 2017.

1305 Ryel R. J., M. M. Caldwell, C. K. Yoder, D. Or, and A. J. Leffler, Hydraulic redistribution in a
1306 stand of *Artemisia tridentata*: evaluation of benefits to transpiration assessed with a simulation
1307 model, *Oecologia* 130: 173–184, 2002.

1308 Schulze E. D., M. M. Caldwell, J. Canadell, H. A. Mooney, R. B. Jackson, D. Parson, R.
1309 Scholes, O. E. Sala, P. Trimborn, Downward flux of water through roots (i.e., inverse hydraulic
1310 lift) in dry Kalahari sands, *Oecologia*, 115:460–462, doi: 10.1007/s004420050541, 1998.

1311 H. J. Schenk and R.B. Jackson, Mapping the global distribution of deep roots in relation to
1312 climate and soil characteristics, *Geoderma*, 126, (1-2), 129-140,
1313 doi:10.1016/j.geoderma.2004.11.018, 2005.

1314 Schenk H.J., The shallowest possible water extraction profile: A null model for global root
1315 distributions, *Vadose Zone J.*, 7, (3), 1119-1124, doi: 10.2136/vzj2007.0119, 2008.

1316 Schlesinger W. H., and S. Jasechko, Transpiration in the global water cycle, *Agr. Forest*
1317 *Meteorol.*, 189 – 190:115 –117, doi:10.1016/j.agrformet.2014.01.011, 2014.

1318 Schymanski, S. J., M. Sivapalan, M. L. Roderick, J. Beringer, and L. B. Hutley, An optimality-
1319 based model of the coupled soil moisture and root dynamics, *Hydrol. Earth Syst. Sci.*, 12, 913-
1320 932, doi: 10.5194/hess-12-913-2008, 2008.

1321 Schnepf A., D. Leitner, M. Landl, G. Lobet, T. H. Mai, S. Morandage, C. Sheng, M. Zörner, J.
1322 Vanderborght, and H. Vereecken; CRootBox: a structural–functional modelling framework for
1323 root systems, *Ann. Bot.*, 121(5), 1033–1053, doi: 10.1093/aob/mcx221, 2018.

1324 Schoppach R., D. Wauthelet, L. Jeanguenin, and W. Sadok, Conservative water use under high
1325 evaporative demand associated with smaller root metaxylem and limited trans-membrane water
1326 transport in wheat, *Functional Plant Biology*, 41(3) 257-269 doi: 10.1071/FP13211, 2013.

1327 Schroder, T., M. Javaux, J. Vanderborght, B. Korfgen, and H. Vereecken, Implementation of a
1328 microscopic soil-root hydraulic conductivity drop function in a three-dimensional soil-root
1329 architecture water transfer model, Vadose Zone J., 8, 783–792, doi: 10.2136/vzj2008.0116,
1330 2009.

1331 Sellers, P. J., D. A. Randall, G. J. Collatz, J. A. Berry, C. B. Field, D. A. Dazlich, C. Zhang, G. D.
1332 Collelo, and L. Bounoua, A revised land surface parameterization (SiB2) for atmospheric GCMs,
1333 1. Model formulation, *J. Clim.* 9, 676–705, doi: 10.1175/1520-
1334 0442(1996)009<0676:ARLSPF>2.0.CO;2, 1996.

1335 Shrestha, P., M. Sulis, M. Masbou, S. Kollet, and C. Simmer, A scale-consistent Terrestrial
1336 Systems Modeling Platform based on COSMO, CLM and ParFlow, *Mon. Wea. Rev.*, 142(9),
1337 3466-3483, doi: 10.1175/MWR-D-14-00029.1, 2014.

1338 Simmer, C., I. Thiele-Eich, M. Masbou, W. Amelung, S. Crewell, B. Diekkrueger, F. Ewert, H.-J.
1339 Hendricks Franssen, A. J. Huisman, A. Kemna, N. Klitzsch; S. Kollet, M. Langensiepen, U.
1340 Loehnert, M. Rahman, U. Rascher, K. Schneider, J. Schween, Y. Shao, P. Shrestha, M.
1341 Stiebler, M. Sulis, J. Vanderborght, H. Vereecken, J. van der Kruk, T. Zerenner, and G.
1342 Waldhoff, Monitoring and Modeling the Terrestrial System from Pores to Catchments - the
1343 Transregional Collaborative Research Center on Patterns in the Soil-Vegetation-Atmosphere
1344 System. *Bull. Am. Meteorol. Soc.*, 96, 1765–1787, doi: 10.1175/BAMS-D-13-00134.1, 2014.

1345 Siqueira, M., G. Katul, and A. Porporato, Onset of water stress, hysteresis in plant conductance,
1346 and hydraulic lift, Scaling soil water dynamics from millimeters to meters, *Water Resour. Res.*,
1347 44, W01432, doi:10.1029/2007WR006094, 2008.

1348 Siqueira, M., G. Katul, and A. Porporato, Soil moisture feedbacks on convection triggers: The
1349 role of soil–plant hydrodynamics, *J. Hydrometeor.*, 10, 96–112, doi:10.1175/2008JHM1027.1,
1350 2009.

1351 Snyder, K. A., J. J. James, J. H. Richards, and L. A. Donovan, Does hydraulic lift or nighttime
1352 transpiration facilitate nitrogen acquisition? *Plant Soil*, 356:159–166, doi: 10.1007/s11104-008-
1353 9567-7, 2008.

1354

1355 Soylu, M. E., S. P. Loheide, and C. J. Kucharik, Effects of Root Distribution and Root Water
1356 Compensation on Simulated Water Use in Maize Influenced by Shallow Groundwater, *Vadose*
1357 *Zone J.* 16. doi:10.2136/vzj2017.06.0118, 2017.

1358 Sperry, J. S., F. R. Adler, G. S. Campbell, and J. P. Comstock, Limitation of plant water use by
1359 rhizosphere and xylem conductance: results from a model, *Plant, Cell & Environment*, 21, 347-
1360 359, doi: 10.1046/j.1365-3040.1998.00287.x, 1998.

1361 Sperry, J. S., U. G. Hacke, R. Oren, and J. P. Comstock, Water deficits and hydraulic limits to
1362 leaf water supply, *Plant, Cell & Environment*, 25: 251–263. doi:10.1046/j.0016-
1363 8025.2001.00799.x, 2002.

1364 Steffen, W., K. Richardson, J. Rockström, S. E. Cornell, I.Fetzer ,E. M. Bennett, R. Biggs, S. R.
1365 Carpenter, W. de Vries, C. A. de Wit, C. Folke, D. Gerten, J. Heinke, G. M. Mace, L. M.
1366 Persson, V. Ramanathan, B. Reyers, and S. Sörlin, Planetary boundaries: guiding human
1367 development on a changing planet, *Science*, 347(6223), 736, doi:10.1126/science.1259855,
1368 2015.

1369 Steudle, E., and C.A. Peterson, How does water get through roots?, *J. Exp. Bot.* 49:775–788.
1370 10.1093/jexbot/49.322.775, 1998.

1371 Tang, J., W. J. Riley, and J. Niu, Incorporating root hydraulic redistribution in CLM4.5: Effects on
1372 predicted site and global evapotranspiration, soil moisture, and water storage, *J. Adv. Model.*
1373 *Earth Syst.*, 7, 1828–1848, doi:10.1002/2015MS000484, 2015.

1374

1375 Tardieu F. and W. J. Davies, Integration of hydraulic and chemical signalling in the control of
1376 stomatal conductance and water status of droughted plants, *Plant, Cell & Environment*, 16(4),
1377 341-349, doi: 10.1111/j.1365-3040.1993.tb00880.x, 1993.
1378
1379 Tardieu F., and T. Simonneau, Variability among species of stomatal control under fluctuating
1380 soil water status and evaporative demand: modelling isohydric and anisohydric behaviours, J.
1381 *Exp. Bot*. 49:419-432, 1998.
1382 Tardieu F., T. Simonneau, and B. Parent, Modeling the coordination of the controls of stomata
1383 aperture, transpiration, leaf growth, and abscisic acid: update and extension of the Tardieu-
1384 Davies model, J. Exp. Bot., 66(8), 2227-2237, doi: 10.1093/jxb/erv039, 2015.

1385 Taylor, K. E., Summarizing multiple aspects of model performance in a single diagram, *J.*
1386 *Geophys. Res.*, 106, 7183– 7192, doi:10.1029/2000JD900719, 2001.

1387 Teuling, A. J., S. I. Seneviratne, R. Stöckli, M. Reichstein, E. Moors, P. Ciais, S. Luyssaert, B.
1388 Van Den Hurk, C. Ammann, C. Bernhofer, E. Dellwik, D. Gianelle, B. Gielen, T. Gruenwald, K.
1389 Klumpp, L. Montagnani, C. Moureaux, M. Sottocornola, G. Wohlfahrt, Contrasting response of
1390 European forest and grassland energy exchange to heatwaves, *Nat. Geosci.* 3, 722–727,
1391 doi:10.1038/ngeo950, 2010.

1392 Topp, G. C., J. L. Davis, and A. P. Annan, Electromagnetic determination of soil water content:
1393 Measurements in coaxial transmission lines, *Water Resour. Res.*, 16(3), 574–582,
1394 doi:10.1029/WR016i003p00574, 1980.

1395 Tyree, M.T., S. Patiño, J. Bennink, and J. Alexander, Dynamic measurements of roots hydraulic
1396 conductance using a high-pressure flowmeter in the laboratory and field, *J. Exp. Bot.* ,46:83–94,
1397 doi:10.1093/jxb/46.1.83, 1995.

1398

1399 Tuzet, A., A. Perrier, R. Leuning, A coupled model of stomatal conductance, photosynthesis and
1400 transpiration, Plant Cell. & Environ. 26, 1097-1116, doi: 10.1046/j.1365-3040.2003.01035.x,
1401 2003.

1402 Van Looy, K., J. Bouma, M. Herbst, J. Koestel, B. Minasny, U. Mishra, C. Montzka, A. Nemes,
1403 Y. A. Pachepsky, J. Padarian, M. G. Schaap, B. Toth, A. Veroef, J. Vanderborght, M. J. van der
1404 Ploeg, L. Weihermüller, S. Zacharias, Y. Zhang, and H. Vereecken, Pedotransfer functions in
1405 Earth system science: Challenges and perspectives, *Rev. Geophys.*, 55, doi:
1406 10.1002/2017RG000581, 2017.

1407 Verhoef, A., and G. Egea, Modeling plant transpiration under limited soil water: Comparison of
1408 different plant and soil hydraulic parameterizations and preliminary implications for their use in
1409 land surface models, *Agric. For. Meteorol.*, 191, 22-32, doi: 10.1016/j.agrformet.2014.02.009,
1410 2014.

1411 Verma P., S. P. Loheide, D. Eamus, and E. Daly, Root water compensation sustains
1412 transpiration rates in an Australian woodland, *Adv. Water Resour.*, 74, 91-101,
1413 10.1016/j.advwatres.2014.08.013, 2014,

1414 Von Storch, H., and F. W. Zwiers, *Statistical Analysis in Climate Research*, 484 pp., Cambridge
1415 Univ. Press, New York,1999.

1416 Warren, J. M., P. J. Hanson, C. Iversen, J. Kumar, A. P. Walker, and S. D. Wullschleger, Root
1417 structural and functional dynamics in terrestrial biosphere models – evaluation and
1418 recommendations, *New Phytol.*, 205: 59-78. doi:10.1111/nph.13034, 2015.

1419 Wells, C., and S. Birchfield, Rootfly: Software for minirhizotron image analysis. College Eng.,
1420 Comput., Appl. Sci., Clemson Univ., Clemson, SC, 2009

1421

Wesseling, J.G., J.A. Elbers, P. Kabat, and B.J. van den Broek. SWATRE: Instructions for input, internal note. Winand Staring Centre, Wageningen, the Netherlands, 1991.

Wright IJ, Reich PB, Westoby M et al., The worldwide leaf economics spectrum. *Nature*, 428, 821–827, 2004.

Williams, M., Y. Malhi, A. Nobre, E. Rastetter, J. Grace, M. Pereira, Seasonal variation in net carbon exchange and evapotranspiration in a Brazilian rain forest: a modelling analysis. Plant Cell & Environ. 21, 953-968, doi: 10.1046/j.1365-3040.1998.00339.x, 1998.

Yan, B., and R. E. Dickinson, Modeling hydraulic redistribution and ecosystem response to droughts over the Amazon basin using Community Land Model 4.0 (CLM4), *J. Geophys. Res.*, 119, 2130–2143, doi:10.1002/2014JG002694, 2014.

Zacharias, S., H. Bogena, L. Samaniego, M. Mauder, R. Fuß, T. Pütz, M. Frenzel, M. Schwank, C. Baessler, K. Butterbach-Bahl, O. Bens, E. Borg, A. Brauer, P. Dietrich, I. Hajnsek, G. Helle, R. Kiese, H. Kunstmann, S. Klotz, J. C. Munch, H. Papen, E. Priesack, H. P. Schmid, R. Steinbrecher, U. Rosenbaum, G. Teutsch, and H. Vereecken, A network of terrestrial environmental observatories in Germany, *Vadose Zone J.*, 10, 955–973, doi: 10.2136/vzj2010.0139, 2011.

Zarebanadkouki M., F. Meunier, V. Couvreur, J. Cesar, M. Javaux, and A. Carminati, Estimation of the hydraulic conductivities of lupine roots by inverse modelling of high-resolution measurements of root water uptake, *Ann. Bot.*, 118(4), 853-864, doi: 10.1093/aob/mcw154, 2016.

1444 Zheng, Z., and G. Wang, Modeling the dynamic root water uptake and its hydrological impact at
1445 the Reserva Jaru site in Amazonia, *J. Geophys. Res.*, 112, G04012,
1446 doi:10.1029/2007JG000413, 2007.

1447 Zhou, S., R. A. Duursma, B. E. Medlyn, J. W. G Kelly, and I. C. Prentice, How should we model
1448 plant responses to drought? An analysis of stomatal and non-stomatal responses to water
1449 stress*, Agr. Forest Meteorol.*, 182/183, 204–214, doi: 10.1016/j.agrformet.2013.05.009, 2013.

1450 Zhu, S., H. Chen, X. Zhang, N. Wei, W. Shangguan, H. Yuan, S. Zhang, L. Wang, L. Zhou, and
1451 Y. Dai, Incorporating root hydraulic redistribution and compensatory water uptake in the
1452 Common Land Model: Effects on site level and global land modeling, *J. Geophys. Res.*., 122,
1453 7308–7322, doi:10.1002/2016JD025744, 2017.

1454

1455